Title

Conserved SMP domains of the ERMES complex bind phospholipids and mediate tether assembly.

Journal

Proceedings of the National Academy of Sciences of the United States of America, 112(25)

ISSN

0027-8424

Authors

AhYoung, Andrew P
Jiang, Jiansen
Zhang, Jiang
et al.

Publication Date

2015-06-01

DOI

10.1073/pnas.1422363112

Peer reviewed

Conserved SMP domains of the ERMES complex bind phospholipids and mediate tether assembly

Andrew P. AhYoung[a], Jiansen Jiang[b,c], Jiang Zhang[d], Xuan Khoi Dang[a], Joseph A. Loo[d,e,f], Z. Hong Zhou[b,c,f], and Pascal F. Egea[a,f,1]

[a]Department of Biological Chemistry, David Geffen School of Medicine, University of California, Los Angeles, CA 90095; [b]Department of Microbiology, Immunology and Molecular Genetics, University of California, Los Angeles, CA 90095; [c]California NanoSystems Institute, University of California, Los Angeles, CA 90095; [d]Department of Chemistry and Biochemistry, University of California, Los Angeles, CA 90095; [e]UCLA–DOE Institute for Genomics and Proteomics, University of California, Los Angeles, CA 90095; and [f]Molecular Biology Institute, University of California, Los Angeles, CA 90095

Edited by Peter Walter, University of California, San Francisco, CA, and approved May 19, 2015 (received for review November 25, 2014)

Membrane contact sites (MCS) between organelles are proposed as nexuses for the exchange of lipids, small molecules, and other signals crucial to cellular function and homeostasis. Various protein complexes, such as the endoplasmic reticulum-mitochondrial encounter structure (ERMES), function as dynamic molecular tethers between organelles. Here, we report the reconstitution and characterization of subcomplexes formed by the cytoplasm-exposed synaptotagmin-like mitochondrial lipid-binding protein (SMP) domains present in three of the five ERMES subunits—the soluble protein Mdm12, the endoplasmic reticulum (ER)-resident membrane protein Mmm1, and the mitochondrial membrane protein Mdm34. SMP domains are conserved lipid-binding domains found exclusively in proteins at MCS. We show that the SMP domains of Mdm12 and Mmm1 associate into a tight heterotetramer with equimolecular stoichiometry. Our 17-Å-resolution EM structure of the complex reveals an elongated crescent-shaped particle in which two Mdm12 subunits occupy symmetric but distal positions at the opposite ends of a central ER-anchored Mmm1 homodimer. Rigid body fitting of homology models of these SMP domains in the density maps reveals a distinctive extended tubular structure likely traversed by a hydrophobic tunnel. Furthermore, these two SMP domains bind phospholipids and display a strong preference for phosphatidylcholines, a class of phospholipids whose exchange between the ER and mitochondria is essential. Last, we show that the three SMP-containing ERMES subunits form a ternary complex in which Mdm12 bridges Mmm1 to Mdm34. Our findings highlight roles for SMP domains in ERMES assembly and phospholipid binding and suggest a structure-based mechanism for the facilitated transport of phospholipids between organelles.

interorganelle tether | phospholipid exchange | membrane contact sites | membrane protein complex | electron microscopy

Eukaryotic cells comprise a complex and interconnected network of membrane-bound organelles. Although this remarkable cellular compartmentalization enables the efficient segregation of diverse metabolic processes, the membranes that envelop these organelles impose a physical barrier impeding the exchange of molecules. To overcome this problem, eukaryotic cells exploit membrane contact sites (MCS), or regions of proximity between two organelles, for the transfer and exchange of cellular signals (1, 2).

With the exception of the endoplasmic reticulum (ER), all organelles lack the biochemical machinery necessary to synthesize a full complement of their phospholipids (3–5). This situation imposes a requirement for interorganelle phospholipid exchange for the biogenesis of organelles, with the principal exporter of these molecules being the ER. Although most organelles obtain their lipids through vesicular trafficking, others, such as mitochondria, are not connected to such pathways and therefore obtain their lipids by nonvesicular mechanisms. Physical connections between the ER and mitochondria at sites called "mitochondria-associated membranes" (MAMs) have been implicated in the nonvesicular transport of lipids (6). However, the molecular mechanisms that govern transport at MAMs are largely unresolved. Growing evidence points to a prospective role for interorganelle tethering complexes in the exchange of phospholipids at MCS (1, 7). These tethers typically comprise soluble and membrane proteins that reside on the surface of the ER and the associated organelle. For contact sites with mitochondria, a multisubunit complex called the "endoplasmic reticulum-mitochondrial encounter structure" (ERMES) has been shown to provide a bridge to the ER in the yeast *Saccharomyces cerevisiae*. The ERMES comprises the soluble protein Mdm12, the ER-resident membrane protein Mmm1, two outer mitochondrial membrane proteins, Mdm10 and Mdm34 (8), and the mitochondrial regulatory Miro GTPase Gem1 (Fig. 1*A*) (9, 10).

The biosynthesis of aminoglycerophospholipids requires the extensive exchange of phospholipid precursors between the ER and mitochondria (5). As depicted in Fig. 1*B* and Fig. S1, the synthesis of phosphatidylcholine (PC) in the ER requires the transport of phosphatidylserine (PS) from the ER to mitochondria to synthesize phosphatidylethanolamine (PE), after which PE is transported back to the ER to produce PC. In the absence of ERMES, the conversion of PS to PC was shown to be impaired (8). Although other studies reported no noticeable change in the conversion of PS to PE (11, 12), these results potentially can be explained by additional cellular mechanisms for phospholipid exchange that can compensate for ERMES

Significance

Phospholipid exchange between the endoplasmic reticulum (ER) and mitochondria is essential for membrane biogenesis and, ultimately, cell survival. It remains unclear, however, how this exchange is facilitated. Our study investigates a putative involvement of the ER-mitochondrial encounter structure (ERMES), a tethering complex that bridges the ER and mitochondria, in phospholipid transport in yeast. We show that a conserved ERMES domain called the "synaptotagmin-like mitochondrial lipid-binding protein" (SMP) domain preferentially binds phosphatidylcholines and mediates the hierarchical assembly of the tether. The 17-Å-resolution EM structure of the complex formed between the SMP domains present in two ERMES subunits, Mdm12 and Mmm1, reveals an elongated, tubular-shaped heterotetramer traversed by a hydrophobic channel, suggesting a mechanism for lipid transport between the two organelles.

Author contributions: A.P.A., J.J., J.A.L., Z.H.Z., and P.F.E. designed research; A.P.A., J.J., J.Z., X.K.D., and P.F.E. performed research; A.P.A., J.J., X.K.D., and P.F.E. contributed new reagents/analytic tools; A.P.A., J.J., J.Z., and P.F.E. analyzed data; and A.P.A., J.J., and P.F.E. wrote the paper.

The authors declare no conflict of interest.

This article is a PNAS Direct Submission.

[1]To whom correspondence should be addressed. Email: pegea@mednet.ucla.edu.

This article contains supporting information online at www.pnas.org/lookup/suppl/doi:10.1073/pnas.1422363112/-/DCSupplemental.

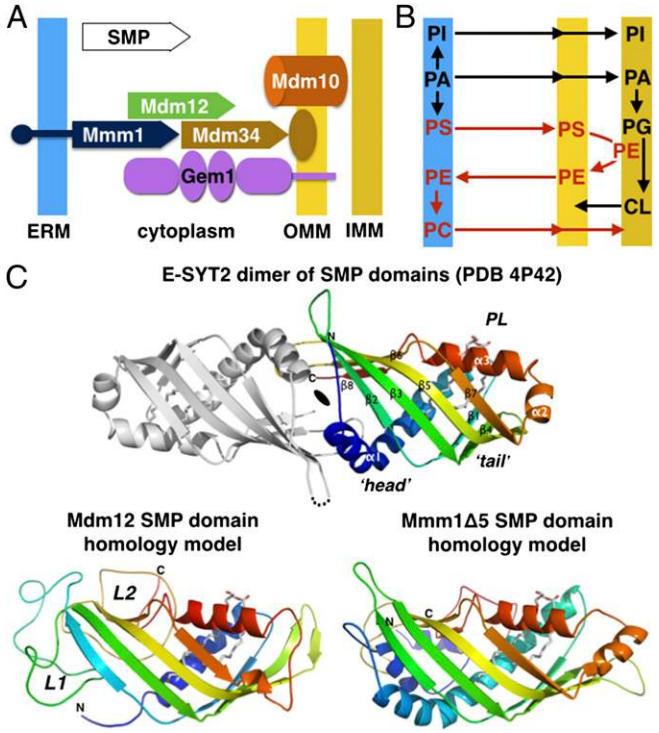

Fig. 1. ERMES, phospholipid metabolism, and the signature SMP domain. (*A*) Subunit topology and composition of the ERMES complex. The three SMP domain-containing subunits Mdm12, Mmm1, and Mdm34 together with a β-barrel outer mitochondrial membrane protein Mdm10 and the calcium-activated regulatory GTPase Gem1 constitute the ERMES in yeast. The SMP domains are depicted with a plain arrow. (*B*) Interconnection of the phospholipid metabolic pathways at the interface between ER and mitochondria. (*C*, *Upper*) Homology models for the SMP domains of yeast Mdm12 and Mmm1. The crystal structure of the head-to-head dimer of SMP domain of E-SYT2 (23) present in an ER-to-plasma membrane tether is shown with the observed bound phospholipid (PL). Only one SMP monomer has been colored. (*Lower*) Phyre[2] homology models of the yeast Mdm12 and Mmm1 SMP. L1 and L2 refer to the nonconserved insertions present in Mdm12 sequences.

function. Consistent with this possibility, two recent studies (13, 14) have identified a second complex called the "vacuole and mitochondria patch" (vCLAMP) that bridges the vacuole and mitochondria, potentially alleviating the loss of ERMES by importing ER-derived lipids from the vacuole to mitochondria. The absence of one causes expansion of the other, whereas the elimination of both is lethal. To date, the direct involvement of ERMES in phospholipid exchange remains inconclusive.

A unique feature of ERMES is the presence of a synaptotagmin-like mitochondrial lipid-binding protein (SMP) domain in three of its five subunits: Mdm12, Mmm1, and Mdm34 (Fig. 1*A*) (15–17). Although the function of the SMP domain is not fully understood, emerging evidence suggests a potential role in lipid transport. SMP-containing proteins are localized predominantly at contact sites between the ER and other organelles (18). They belong to the tubular lipid-binding protein (TULIP) superfamily comprising known lipid-binding proteins such as Takeout (19), the bactericidal/permeability-increasing protein (BPI) (20), the cholesteryl ester transfer protein (CETP) (21), and the lipopolysaccharide-binding protein (LBP) (22). The crystal structure of the SMP domain of the human extended synaptotagmin 2 protein (E-SYT2) was determined recently (23), revealing its tubular structure with a hydrophobic tunnel occupied by a phospholipid (Fig. 1*C*). These structural features resemble other TULIP proteins, suggesting that the SMP domain has a conserved physiological role in phospholipid binding and transport.

Important advances have been made in establishing the importance of ERMES in membrane tethering. However, we still lack basic knowledge of how the structural properties of ERMES constituents (i.e., subunit structure and stoichiometry) are related to the function of the complex. To help bridge this gap, we combined computational modeling, analytical biochemistry, MS, quantitative lipidomics, and EM to elucidate the role of the conserved SMP domain as a key component of ERMES. Here, we report the first structure, to our knowledge, of a subcomplex of ERMES, revealing a unique mode of assembly between the SMP domains of Mdm12 and Mmm1. We also demonstrate that Mdm12 bridges Mmm1 and Mdm34, providing a structural basis for membrane tethering. Last, the SMP domain binds phospholipids, supporting the direct involvement of ERMES in phospholipid exchange. Our results lay the groundwork for future structural and functional dissections of ERMES and other interorganelle tethering complexes in yeast and mammals.

Results

Homology Modeling and Sequence Analysis of the SMP Domains of Mdm12 and Mmm1 Reveal Conserved Folds and Surfaces. In yeast, Mdm12 is a soluble protein, and Mmm1 is an ER membrane protein with an N-terminal glycosylated luminal extension, a single transmembrane α-helix, and a large cytoplasmic C-terminal domain. Previous bioinformatics studies predict that the SMP domain of Mdm12 spans the full-length protein (residues M1–E271), and that of Mmm1 maps to its C terminus at residues E196–P409 (16, 17). On the other hand, the SMP domain of Mdm34 is N-terminal and is followed by a region predicted to be disordered and presumably involved in the association with the outer mitochondrial membrane (Fig. S2 *A* and *B*). Based on this prediction, we considered the full-length Mdm12 and an SMP-containing fragment of Mmm1 (residues K162–L426, termed "Mmm1Δ5") for modeling with Phyre[2] (*SI Experimental Procedures*) (24). Comparative homology modeling of the two SMP domains using structures of proteins in the Protein Data Bank (PDB) identified the SMP domain of human E-SYT2 (23) as the best template; other members of the TULIP superfamily, including BPI, CETP, and LBP, also were identified as suitable templates.

The SMP domain of E-SYT2 forms a dimer in which each monomeric unit comprises an incomplete, but highly twisted, seven-stranded β-barrel and three helices (α1, α2, and α3), with α2 partially capping one end of the barrel (Fig. 1*C*). Like all TULIP proteins, the internal lipid-binding cavity of E-SYT2 is lined with hydrophobic residues. Despite the overall low sequence identity (~16–18%) between E-SYT2 and Mdm12 or Mmm1Δ5, the two ERMES proteins were modeled with greater than 90% confidence (Fig. S3). The two models closely resemble the E-SYT2 structure; the core rmsd between the SMP model of Mdm12 or Mmm1 and the template E-SYT2 crystal structure is ~1 Å (Figs. 1*C* and 2*A* and Fig. S3*A*). The elongated feature of these models is particularly pronounced in the case of Mdm12; in both Mdm12 and Mmm1 the internal cavity is lined with hydrophobic residues and has dimensions, geometries, and chemical properties compatible with the binding of hydrophobic ligands such as phospholipids (Fig. 2*B*).

Next, we analyzed the amino acid sequence conservation of Mdm12 or Mmm1 by multiple sequence alignments using 21 fungal and five nonfungal orthologs in organisms in which a full complement of ERMES proteins had been annotated (25). The resulting scores were mapped to the protein surfaces of our homology models using ConSurf (26) (*SI Experimental Procedures*) to highlight conserved structural features of the two proteins. This comprehensive analysis revealed two conserved surfaces near residues S2–W7 and N142–F148 of Mdm12 and two

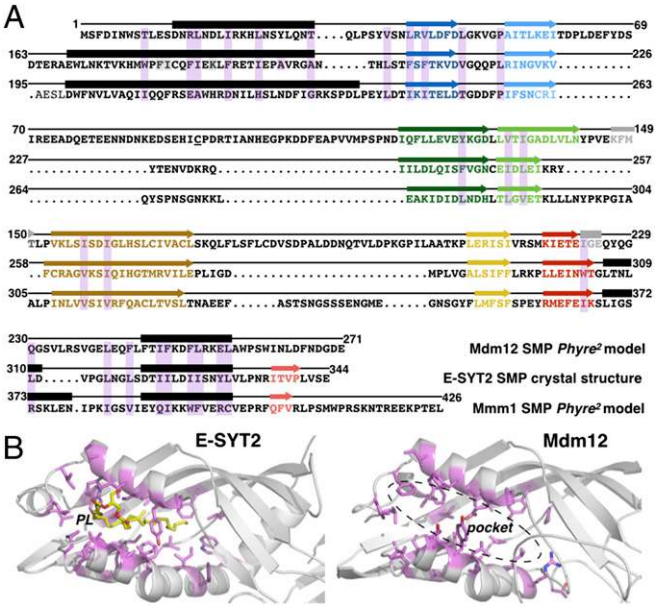

Fig. 2. The predicted hydrophobic binding pockets of Mdm12 and Mmm1 SMP domains resemble that of E-SYT2. (*A*) Alignment of Mdm12 and Mmm1 amino acid sequences to E-SYT2 using predicted structural homology. The structures of the SMP domains of Mdm12 and Mmm1 (Phyre^2 homology models) and E-SYT2 (crystal structure) were superposed to identify residues (shaded in magenta) of Mdm12 and Mmm1 equivalent in terms of position to those involved in phospholipid binding in E-SYT2. α-Helices and β-strands are depicted as black rectangles and colored arrows, respectively. (*B*) The binding pockets of the SMP domain of E-SYT2 and Mdm12. Equivalent residues (magenta) involved in phospholipid binding in E-SYT2 are mapped on the Mdm12 structure. The bound phospholipid (yellow) is shown in E-SYT2; the corresponding pocket in Mdm12 is hydrophobic and of similar dimensions.

conserved surfaces near residues E196–N202–Q207 and R373–L376–K381 of Mmm1. The conserved regions appeared to be located on the opposite ends ("head" and "tail") of the elongated, tubular-shaped SMP domains (Figs. S3*A* and S4*A*). Because the SMP domain of E-SYT2 forms a homodimer, we also modeled the corresponding assemblies in Mmm1 and Mdm12. Our analysis suggests that the SMP domain of Mmm1 displays structural features compatible with the formation of a similar homodimer (Fig. S4*B*). In such a configuration, the two 45-Å-long tubular SMP domains would associate head-to-head to form a 90-Å-long cylinder.

The SMP Domains of Mdm12 and Mmm1 Form a Tight Heterotetramer with Equimolecular Stoichiometry. We hypothesized that the cytoplasm-exposed SMP domains of ERMES subunits mediate their assembly into a molecular tether. To test this, we explored the propensity for complex formation by the SMP domains of Mdm12 and Mmm1. Based on previous bioinformatics predictions (16) and our homology models, we proceeded to isolate a soluble SMP-containing fragment of Mmm1 using a systematic deletion strategy by which eight deletion constructs (termed "Mmm1Δ1" through "Mmm1Δ8") (Fig. S2*A*) that mapped along the cytoplasmic-exposed region of Mmm1 were generated. The Mmm1Δ1 construct encoded the full cytoplasmic domain (S122–L426) of Mmm1, whereas Mmm1Δ2 to Mmm1Δ8 encoded truncated variants in which 10 amino acids were successively deleted from the N terminus of Mmm1Δ1. The constructs displayed varied levels of expression and solubility when expressed and purified from *Escherichia coli*. However, these levels improved substantially when the proteins were fused at their N termini to a thrombin-cleavable, maltose-binding protein (MBP-Mmm1Δ1–Δ8). Unlike the other constructs, Mmm1Δ8 remained largely insoluble with no improvement in solubility when fused to MBP.

Next, we tested for complex formation by coexpressing full-length Mdm12 with three MBP-Mmm1 constructs: MBP-Mmm1Δ1, MBP-Mmm1Δ5, and MBP-Mmm1Δ7 (Fig. 3*A*). The resultant fusion complexes were isolated by affinity chromatography using the His_6 tag on Mmm1 (Mdm12 was not tagged). Subsequent purification by size-exclusion chromatography (SEC) revealed the formation of a stable and monodisperse complex for all three combinations tested (Fig. 3 *B* and *C* and Fig. S5*A*). Upon treatment with thrombin, we observed the quantitative release of the MBP tag, but the resultant complex severed from MBP remained intact. When we coexpressed Mdm12 and Mmm1Δ5 lacking the MBP tag, we observed an identical complex eluting at the same position on SEC as the Mdm12/Mmm1Δ5 severed from MBP (Fig. 3 *B* and *C* and Fig. S5*A*), suggesting that the MBP did not alter the oligomeric assembly of the complex.

We explored the possibility that the solubility, or rather the overall stability, of Mmm1Δ8 might be enhanced by the presence of Mdm12. Thus, we coexpressed Mmm1Δ8 (with or without an MBP tag) and Mdm12. We did not observe the formation of a stable and monodisperse complex, suggesting that Mmm1Δ7 contains the minimal structural elements required for Mmm1 interaction with Mdm12.

We proceeded to determine the stoichiometry of the Mdm12/Mmm1Δ5 complex using SEC coupled to multiangle static light scattering (SEC-MALS), a technique for determining the absolute molar mass of macromolecules in solution (*SI Experimental Procedures*). Our analysis revealed that Mdm12 is a monomer with a mass of ∼31 kDa (Fig. 3*D*), whereas Mdm12/Mmm1Δ5 forms a complex with a mass of ∼133 kDa, compatible (Fig. 3*D*) with a tetrameric arrangement (calculated mass ∼125 kDa). Given the similar molecular mass of Mdm12 and Mmm1Δ5 (∼31.2 kDa), we resolved the ambiguity in subunit stoichiometry by determining the mass of the same complex fused to MBP (MBP-Mmm1Δ5/Mdm12) to be ∼210 kDa (Fig. 3*E*); the increase in mass by ∼77 kDa compared with the MBP-free complex corresponded to the addition of two molecules of MBP (calculated mass ∼41.2 kDa), suggesting that Mdm12 and Mmm1 form a heterotetramer with 2:2 stoichiometry. SEC-MALS also revealed that MBP-Mmm1Δ5 forms dimers (Fig. 3*D*); because MBP is a monomer in solution, the observed dimer could only be the result of interactions between SMP domains, as is consistent with our homology models.

Taken together, our systematic truncation and coexpression strategies enabled the identification and reconstitution of a minimalistic complex of Mdm12/Mmm1 that is mediated by their SMP domains. Most importantly, we observed that Mdm12/Mmm1Δ1, the full cytoplasmic portion of Mdm12/Mmm1, behaves identically to Mdm12/Mmm1Δ5 or Mdm12/Mmm1Δ7 complexes, demonstrating that amino acids 122–181 are not essential for complex formation (Fig. S5*B*). To assemble the complex, a dimer of Mmm1 recruits two monomers of Mdm12.

Mdm12 Acts as a Bridge Between Mmm1 and Mdm34. Having established the existence of a stable subcomplex between the SMP domains of Mdm12 and Mmm1, we investigated the role of the SMP domain of Mdm34 (hereafter termed "Mdm34-SMP") in the assembly of the tether. We expressed Mdm34-SMP (a 22-kDa protein) fused to GFP or GST at its N terminus (GFP is purely monomeric, whereas GST is dimeric) (*SI Experimental Procedures* and Fig. S2*A*). The purified fusion proteins eluted at the same position on SEC, suggesting that Mdm34-SMP is a dimer (Fig. 4*A*). Consistently, Mdm34-SMP generated by controlled intracellular proteolytic processing (*SI Experimental Procedures*) purifies as a dimer on SEC. Previous studies have shown that full-length Mdm34 coimmunoprecipitates with all ERMES components (9, 27). However, the hierarchy of interactions between ERMES

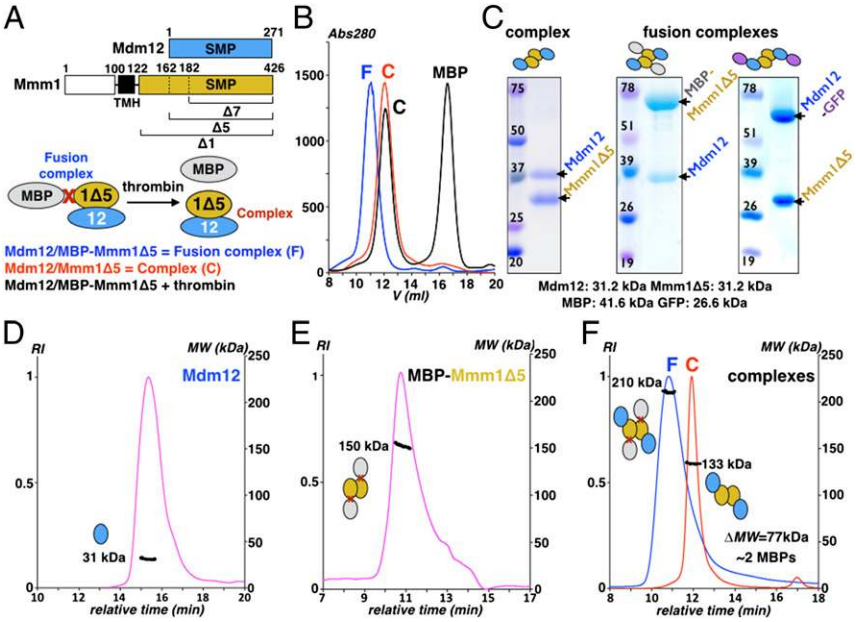

Fig. 3. Reconstitution and characterization of the ERMES Mdm12/Mmm1 heterotetramer. (*A*) Organization of Mdm12 and Mmm1 (*Upper*) and strategy used to coexpress and copurify Mdm12 associated to an MBP-Mmm1Δ construct as a fusion complex (*Lower*). (*B*) Reconstitution of the Mdm12/Mmm1Δ5 complex. Thrombin treatment of the fusion complex releases the monomeric MBP carrier protein from the Mdm12/Mmm1 complex assembled in vivo. The Mdm12/Mmm1Δ5 complex obtained after quantitative removal of the MBP fusion partner is identical to the native Mdm12/Mmm1Δ5. (*C*) Coomassie-stained SDS/PAGE gel of complexes Mdm12/Mmm1Δ5, Mdm12/MBP-Mmm1Δ5, and Mdm12-GFP/Mmm1Δ5 expressed and reconstituted in *E. coli*. These samples also were used for the EM study. (*D–F*) Determination of the mass of Mdm12 (*D*), the MBP-Mmm1Δ5 (*E*), and the Mdm12/MBP-Mmm1Δ5 fusion and Mdm12/Mmm1Δ5 complexes (*F*) by SEC-MALS. Mdm12 is a monomer (31 kDa), whereas MBP-Mmm1Δ5 forms a homodimer (150 kDa). The difference in mass of 77 kDa, measured between the fusion (210 kDa) and the native (133 kDa) complexes, corresponds to two MBP proteins (40 kDa each).

subunits and how these interactions are mediated has never been characterized. To study these interactions in detail, we performed pull-downs using purified His-tagged Mdm34-SMP as bait against Mdm12, the SMP domain of Mmm1 (Mmm1Δ5), or the Mdm12/Mmm1Δ5 complex (Fig. 4*B*). Although Mdm34-SMP interacted with Mdm12 and the Mdm12/Mmm1Δ5 complex, we did not detect any interaction with Mmm1Δ5, suggesting that Mdm12 bridges the SMP domains of Mmm1 and Mdm34. Attempts to stabilize the ternary complex to define its stoichiometry were unsuccessful, likely because of the weak association between Mdm34-SMP and the Mdm12/Mmm1 complex and the propensity of Mdm34-SMP to aggregate.

Within ERMES, Mdm34 and Mmm1 are the only SMP-containing subunits that are membrane anchored; based on our biochemical data, we can propose several models of SMP assemblies that could support apposition of membranes (Fig. 4*C*). The simplest model predicts that two monomers of Mdm12 would bridge the dimers of Mdm34 and Mmm1 (model 1 in Fig. 4*C*); another possibility would consist of two dimers of Mdm34, each contacting one of the two monomers of Mdm12 associated with the Mmm1 dimer (model 2 in Fig. 4*C*). Last, in a more sophisticated model, a dimer of Mdm34 would engage two monomers of Mdm12 projecting from two different and adjacent Mmm1 dimers (model 3 in Fig. 4*C*); this model could explain the observation that in yeast hundreds of ERMES molecules concentrate in punctate structures (8, 28). Although different, each of the resulting SMP assemblies would display some level of symmetry.

The SMP Domains of Mdm12 and Mmm1 Bind Phospholipids. Given the extensive lipid exchange that occurs between the ER and mitochondria and the identification of a phospholipid molecule bound to the SMP domain of E-SYT2, we hypothesized that the SMP-containing subunits of ERMES also may bind phospholipids. To test this hypothesis, Mdm12, Mmm1Δ1, Mmm1Δ5, and their corresponding reconstituted complexes were expressed in *E. coli*, extensively purified to remove any unbound or weakly associated lipid contaminants, and analyzed by quantitative electrospray ionization MS (ESI-MS) and high-performance TLC (HPTLC) for bound phospholipids (*SI Experimental Procedures*).

MS analysis under nondenaturing conditions (native-MS) of Mdm12 purified from *E. coli* revealed the presence of a predominantly ligand-bound form with a mass-to-charge ratio (*m/z*) of 2,653 for charge state +12 and an *apo* form at an *m/z* of 2,588 (Fig. 5*A*). Deconvolution of the spectrum indicated an average difference in mass of ∼703–781 Da between the ligand-bound form (∼31,850 Da) and the *apo* form (∼31,069 Da) of Mdm12, suggesting the presence of a singly-bound molecule of phospholipid per protein (Fig. 5*A*, *Inset*).

To confirm this result, the bound lipids were extracted and analyzed by HPTLC. We identified PE and phosphatidylglycerol (PG) as the primary phospholipids copurifying with Mdm12 (Fig. 5*B*). The molecular identities of these lipids were characterized further by quantitative ESI-MS. Of the bound lipids, 80% were PE species [the most prominent of which is PE (33:1) with an *m/z* of 704.5], and 15% were PG species [the main one being PG (34:1) with an *m/z* of 766.5] (Fig. S6 *A* and *B* and Table S1). The ratio of bound PE to bound PG is consistent with previous lipidomic analyses of bacterial membranes (29) and with our own quantification of total bacterial PE (∼85%) and PG (∼10%) levels (Fig. S6*A*). Correspondingly, we observed the copurification of PE and PG with Mmm1Δ1, Mmm1Δ5, and the corresponding Mdm12/Mmm1 complexes (Fig. 5*B* and Fig. S5*B*). Thus, like Mdm12, the SMP domain of Mmm1 and the reconstituted Mdm12/Mmm1 complexes bound bacterial PE and PG.

A previous bioinformatics and MS-based study demonstrated that ERMES also is present in eukaryotic lineages outside Fungi (25). Thus, we proceeded to corroborate our findings in *S. cerevisiae* by investigating the phospholipid-binding properties of Mdm12 in the closely related *Saccharomyces castellii* and the more distantly

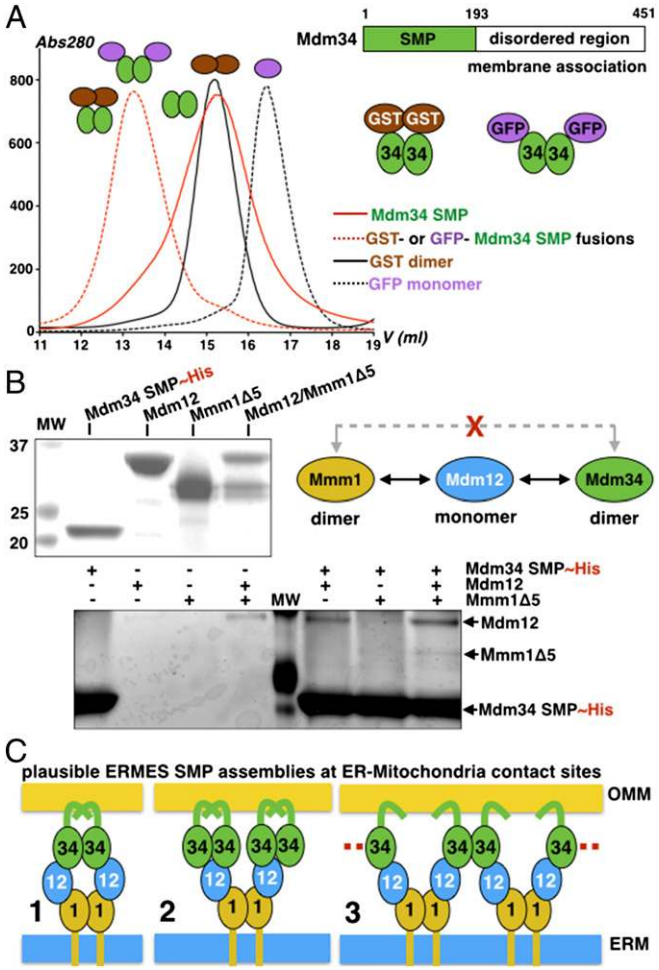

Fig. 4. The SMP domain of Mdm34 interacts with Mdm12 and the Mdm12/Mmm1 complex but not with Mmm1. (*A*) Organization of Mdm34. Strategy used to purify Mdm34 as a GST or a GFP fusion. SEC analysis of the GST and GFP fusion proteins of SMP Mdm34 and comparison with free monomeric GFP (26 kDa) and dimeric GST (2 × 26 = 52 kDa). The SMP domain of Mdm34 (22 kDa) is a dimer. (*B*) Pull-down assay analysis of the interactions between Mdm34 and Mdm12, MBP-Mmm1Δ5, or the Mdm12/Mmm1Δ5 complex. The upper gel shows the proteins used for the pull-down in the lower gel (elutions). Mdm12 bridges Mmm1 to Mdm34. (*C*) Three plausible modes of association among the three SMP domains of ERMES at ER to mitochondria contact sites.

related amoeba, *Dictyostelium discoideum*. Proteins were expressed in *E. coli* (*SI Experimental Procedures*) and analyzed by HPTLC. Binding to bacterial PE and PG was observed in Mdm12 from both species (Fig. 6*A*). So far the limited stability of the Mdm34-SMP prevents the thorough characterization of its lipid-binding properties; nevertheless, sufficient evidence on other SMP-containing proteins strongly supports the possibility that Mdm34 also could bind phospholipids.

Taken together, our data strongly suggest that phospholipid binding is an evolutionarily conserved feature of the SMP domain and therefore implicate ERMES in the direct exchange of phospholipids between the ER and mitochondria.

Mdm12 and Mmm1 Preferentially Bind Phosphatidylcholines. In an attempt to determine the identity of a native phospholipid ligand of Mdm12 or Mmm1, we first tested the ability of purified phospholipids to displace a fluorescently labeled PE, 7-nitrobenz-2-oxa-1,3-diazol-4-yl-1,2-dipalmitoyl-sn-glycero-3–phosphoethanolamine (NBD)-PE, preloaded in Mdm12 purified from *E. coli* (*SI Experimental Procedures* and Fig. 5*C*). The same approach was used to characterize the phospholipid-binding properties of E-SYT2 (23). The phospholipids tested here have fatty acid chain lengths of 16–18 carbons and critical micelle concentrations (CMCs) estimated to be in the nanomolar range. To ensure that the competing phospholipids did not aggregate, we performed this assay in the presence of the detergent lauryldimethylamine-oxide (LDAO). LDAO was chosen for its ability to enhance NBD-PE preloading (presumably by reducing phospholipid aggregation) and its inability to displace NBD-PE already bound to Mdm12 (Fig. S7). We observed an ∼2.7 fold increase in NBD-PE loading in the presence of LDAO at 0.2 mM, twice its CMC compared with the control without detergent (Fig. 5*C* and Fig. S7*A*). Importantly, when we incubated Mdm12 already preloaded with NBD-PE with the same concentration of LDAO, a minimum displacement (less than 10%) was observed (Fig. 5*C* and Fig. S7*B*). Other detergents, such as 3-[(3-Cholamidopropyl)dimethylammonio]-1-propanesulfonate (CHAPS) and lysofoscholine-10 (LFC10), were efficient in NBD-PE loading (Fig. S7 *A–C*); however, when mixed with the purified phospholipids the resulting mixed micelles adversely altered protein migration on blue native PAGE (BN-PAGE). Therefore LDAO was selected as the best candidate.

Mixed micelles containing one given phospholipid (present in 18-molar excess relative to Mdm12) and the noncompeting detergent LDAO (at 0.2 mM final concentration) then were used to examine the phospholipid-binding preference of Mdm12. PE, PC, and PG robustly displaced NBD-PE from Mdm12, achieving 93, 94, and 95% displacement, respectively, as evidenced by the loss of fluorescence in the band corresponding to Mdm12 on BN-PAGE (Fig. 5*C*). Conversely, we observed moderate displacement (∼27%) by phosphatidylinositol (PI) and almost no displacement (less than 5%) by PA, PS, and cardiolipin (Fig. 5*C*). Given the ability of phospholipids to partition into a complex phase composed of free phospholipid, micelles, aggregates, and also mixed micelles in the presence of detergent, it is not possible to quantify the binding affinity between Mdm12 and phospholipids accurately. Phospholipids remain bound to the recombinant proteins despite extensive purification (i.e., four to five chromatographic steps), suggesting a relatively high binding affinity.

PE, PC, PG, and, to a lesser extent, PI bind to Mdm12, but PA, PS, and cardiolipin (CL) do not. In nonphotosynthetic eukaryotes, such as yeast and mammals, PG is synthesized only in the inner mitochondrial membrane where it is used as a precursor for cardiolipin biosynthesis (4, 5). The nearly complete displacement observed for PG is puzzling, because its reported cellular localization precludes contact with Mdm12 and other ERMES components. However, all the other lipids are accessible to binding by ERMES subunits based on their distribution in ER and outer mitochondrial membranes (30). Based on the E-SYT2 structure, the SMP domain of Mdm12 probably interacts primarily with the acyl chains of phospholipids. Our data indeed demonstrate that Mdm12 promiscuously binds some glycerophospholipids but also highlight its ability to discriminate against others. These results suggest the presence of cryptic determinants for selective lipid recognition.

In parallel with the lipid displacement assay described above, we sought to identify the bona fide endogenous ligand of the SMP domain by analyzing the lipids bound to Mdm12 purified from yeast, its native host (Fig. 6*A*). HPTLC revealed the presence of PC and likely a mixture of PE and PI (which comigrate on the TLC plate). We confirmed this finding by ESI-MS, which revealed the presence of PC (60%), PI (23%), PE (10.5%), and a small amount of PS (3%) (Fig. 6*B*). PC is absent in most bacterial species, including *E. coli* (29), explaining why it was not detected in our previous experiments. The total cellular phospholipid levels present in yeast containing overexpressed levels of Mdm12 are very similar to previously reported yeast phospholipid levels

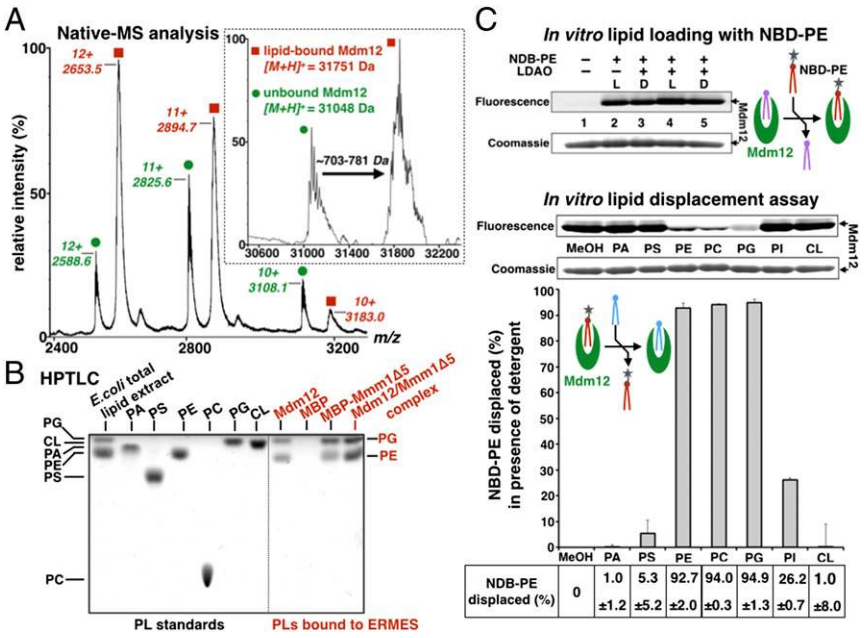

Fig. 5. Mdm12, Mmm1, and their complex bind phospholipids promiscuously. (*A*) Native-MS analysis of yeast Mdm12 expressed in *E. coli*. Yeast Mdm12 purified from *E. coli* copurifies with noncovalently bound ligands with a mass ranging from ~703–781 Da. The *Inset* represents the deconvolution of the raw data. (*B*) Mdm12, Mmm1, and the Mdm12/Mmm1 complex bind phospholipids PE and PG. HPTLC of phospholipids extracted from yeast Mdm12 and Mdm12/Mmm1Δ5 complex purified from *E. coli*. Standards of bacterial polar lipid extract and pure phospholipids are run next to the phospholipid extracted from purified yeast Mdm12 and Mdm12/Mmm1Δ5 complex. For Mmm1Δ5, the more stable MBP-Mmm1Δ5 fusion was used. As a negative control, we did not detect any phospholipid bound to MBP. (*C*) In vitro lipid displacement assay showing that PC binds to Mdm12. Purified Mdm12 can be preloaded with fluorescent PE (NBD-PE) as observed by BN-PAGE. Loading of NBD-PE is enhanced by the detergent LDAO. Seven different phospholipids (at 18-fold molar excess) are incubated with Mdm12 preloaded with NBD-PE in the presence of LDAO. MeOH, methanol-only control for the preloaded protein without added competitor phospholipid. NBD-PE displacement percentages are quantified. PE, PC, and PG nearly quantitatively displace the fluorescent PE preloaded in Mdm12. For comparison, the lipid displacement assay performed in absence of detergent is shown in Fig. S7*D*.

(31–34). Interestingly, bound PC (60%) is enriched by at least twofold compared with its natural abundance (~27%). This observation is consistent with the results of our lipid-displacement assay and thus raises the strong possibility that PC might be the main endogenous ligand of Mdm12. The molecular identities of the bound PC species were determined also (Fig. 6*B*, Fig. S6*C*, and Table S1); the most prominent species detected was PC (32:2) with an *m*/*z* of 730.5. Despite the strong affinity of PG for Mdm12 observed in our displacement assays, yeast-purified Mdm12 was not enriched for PG (Fig. 6 *A* and *B*), suggesting that Mdm12 does not bind PG in vivo.

Last, we proceeded to identify the endogenous ligand of Mmm1 and the Mdm12/Mmm1 complex by incubating *E. coli*-purified MBP-Mmm1Δ5 or Mdm12/Mmm1Δ5 complex with liposomes prepared with yeast phospholipids (*SI Experimental Procedures* and Fig. 6*C*). As a positive control, we carried out the same analysis using Mdm12 alone. The use of purified liposomes with defined compositions greatly reduces the possibility of Mdm12 or Mmm1 binding freely existing phospholipid monomers. Here, to bind phospholipids, the proteins must extract them physically from the bilayer environment of the liposomes. HPTLC analysis of lipids extracted from the MBP-Mmm1Δ5 and Mdm12/Mmm1 complex protein samples before and after incubation with liposomes revealed PC and PI displacement of bacterial PE and PG, consistent with our lipid-profiling data on Mdm12 (Fig. 6*C*). Although we observed PI binding to both proteins in this liposome assay, the lack of enrichment in Mdm12 purified from yeast suggests it might not be the main ligand of Mdm12.

Our results from four different experimental approaches show that the SMP domains of Mdm12 and Mmm1are genuine lipid-binding proteins with a preference for phosphatidylcholines.

The Architecture of the Mdm12/Mmm1 Complex Revealed by EM. Reconstituted Mdm12/Mmm1Δ5 and Mdm12/Mmm1Δ1 complexes were examined by negative staining EM (*SI Experimental Procedures*). Class averages of negatively stained particles for both complexes revealed similar elongated, crescent-shaped particles in high homogeneity (Fig. 7*A* and Fig. S8 *A* and *B*). To obtain the 3D structures of these complexes, we first performed 3D reconstruction of the Mdm12/Mmm1Δ5 complex using the random conical tilt (RCT) method (Fig. S8*E*) (35), which can generate 3D maps from tilt-pair images without the need of an initial 3D model. The RCT 3D reconstruction of the Mdm12/Mmm1Δ5 complex yielded an EM map at 35-Å resolution (Fig. 7*D* and Fig. S8*D*) that displayed structural features consistent with the class averages. Interestingly, even though no symmetry was applied during the 3D reconstruction, the EM map shows strong features of twofold rotational symmetry. Next, we reconstructed the 3D EM map of the Mdm12/Mmm1Δ1 complex to 17-Å resolution from negatively stained particle images using the aforementioned RCT 3D EM map of the Mdm12/Mmm1Δ5 complex as the initial model and with a twofold symmetry applied (Fig. 7*E* and Fig. S8*D*). Except for the difference in resolution, the reconstructions obtained the two complexes are highly similar, indicating that the two complexes adopt a relatively homogeneous and similar architecture and conformation (Fig. 7 *D* and E). Overall, the Mdm12/Mmm1 complex is crescent-shaped and exhibits twofold symmetry. With dimensions of ~210 × 45 × 35 Å along the three major axes, anisotropy is the most salient structural feature of the complex.

To locate the positions of both Mdm12 and Mmm1 subunits within the 3D structures, we also imaged the complexes with either an MBP tag on the N terminus of Mmm1Δ5 or a GFP tag on the C terminus of Mdm12 (Figs. 3*C* and 7 *B* and *C* and Fig. S8*C*).

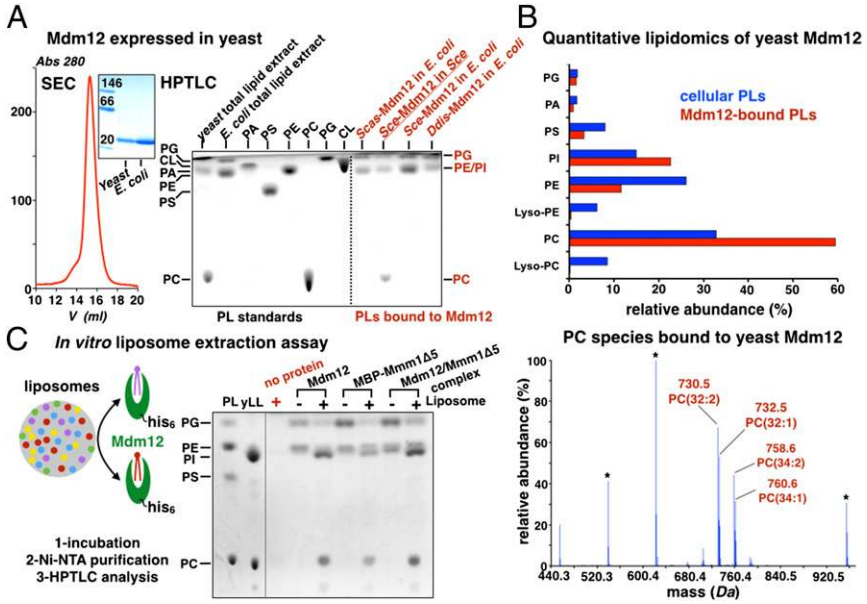

Fig. 6. Phosphatidylcholines are bona fide ligands of Mdm12 and Mmm1. (*A*) Yeast Mdm12 purified from yeast is monomeric and binds PC, PE, and PI. SEC profile of Mdm12 purified from yeast. In BN-PAGE of yeast purified from yeast or *E. coli*, the two proteins are monomeric and undistinguishable. HPTLC analyses of three different Mdm12 proteins from *S. cerevisiae* (*Sce*), *S. castellii* (*Scas*), and the amoeba *D. discoideum* (*Ddis*). All three proteins expressed in *E. coli* contain PE and PG. Mdm12 purified from its native source (yeast) contains PC, PE, and PI. (*B*) Lipid profiling by ESI-MS of yeast Mdm12 purified from yeast shows that Mdm12 preferentially binds to PCs in vivo. (*Upper*) Comparison between the levels of phospholipids (PLs) bound to Mdm12 purified from yeast (red bars) and overall phospholipid levels in yeast (blue bars) showing at least twofold enrichment of PC bound to Mdm12. (*Lower*) The ESI-MS spectrum reveals the PC species bound to Mdm12. The main PC species is PC(32:2) at *m/z* 730.5. Lyso-PCs do not bind. (*C*) In vitro liposome-binding assay to determine the bona fide phospholipid ligands of Mdm12, Mmm1, and their complex. Liposomes prepared with yeast total polar lipid extract (yLL) are incubated with purified His-tagged ERMES proteins (Mdm12, Mmm1Δ5, or their complex). After incubation with liposomes, proteins were purified on nickel-nitrilotriacetic acid (Ni-NTA), and their lipid content was analyzed by HPTLC. The phospholipid contents of proteins incubated (+) or not (–) with liposomes are shown together with a liposome-only control (no protein) showing that no liposome carryover contaminates the protein samples. A phospholipid standard is shown.

Class averages of the tagged complexes clearly revealed additional structures corresponding to either two MBP or two GFP molecules. These findings corroborated the stoichiometry of the complex that we determined biochemically and provided novel structural insights into the spatial organization of Mdm12 and Mmm1Δ5, in which two Mdm12 molecules bind either end of a central Mmm1Δ5 homodimer to form an extended and overall crescent-shaped complex. For the Mdm12/MBP-Mmm1Δ1 complex, although raw particle images show the densities corresponding to each MBP, their density is blurred out after class averaging, thus indicating that they occupy different positions and suggesting that the linker region (S122–L181) in Mmm1 is flexible and contributes little, if any, to the overall architecture of the complex.

The resulting EM maps were used for fitting the crystal structure of the E-SYT2 SMP domain. The E-SYT2 SMP dimer (Fig. 1*C*) was fitted in the central module of the EM structure to model the Mmm1 homodimer, and two E-SYT2 SMP monomers were adjusted separately to model the two distal copies of Mdm12 bound at the symmetric ends of the Mmm1 dimer (Fig. 7 *F* and *G* and Movie S1). We also used our homology models of the Mmm1 homodimer (Fig. S4*B*) and the Mdm12 monomer (Fig. 1*C*) to generate a corresponding pseudoatomic homology model (Movie S2) of the ERMES Mdm12/Mmm1 complex. In our models, the positions of the C terminus of Mdm12 and N terminus of Mmm1 agree with the relative positions of the MBP or GFP based on class averages of the fusion complexes (Fig. S9). Our models also predict a tail-to-head arrangement at the Mmm1-to-Mdm12 interface (Fig. S3) where the SMP domains of Mmm1 and Mdm12 interact through conserved surfaces located at their extremities in agreement with our surface conservation analyses (Fig. S4*A*). In our EM structure, the four tubular SMP domains are nearly aligned; the phospholipid binding cavities present in each SMP domain could rearrange to create one large and quasi-continuous hydrophobic tunnel for channeling lipids between the ER and mitochondria.

Discussion

Our study reveals two important properties of the SMP domains of ERMES: They bind to phospholipids and mediate the physical interactions between Mmm1, Mdm12, and Mdm34. The identification of lipids bound to the SMP domains of Mdm12, Mmm1, and orthologs of Mdm12 that include the distantly related amoeba *Dictyostelium* suggests a conserved physiological lipid-binding role of SMP-containing proteins that is not yet fully understood. One attractive hypothesis that explains the current findings is that these proteins function as lipid transfer proteins (LTP). This hypothesis is supported by the structural similarities of the SMP to proteins in the TULIP superfamily, several of which participate in lipid transfer (21, 36). Moreover, the presence of SMP-containing proteins at ER–mitochondria contact sites (16, 37), which are highly enriched in lipid-synthesizing enzymes (6), strongly supports a role for ERMES in the transfer of lipids.

We demonstrate that the SMP domains of Mdm12 and Mmm1 are capable of binding different glycerophospholipids. Interestingly, the analysis of lipids extracted from Mdm12 purified directly from its native host yeast demonstrated that there was substantial enrichment of PC compared with other phospholipids. Consistently, when Mdm12 or the SMP domain of Mmm1 purified from *E. coli* was incubated with liposomes prepared with yeast phospholipids, it was evident that PC, and to some extent PI, strongly displaced bacterial PE and PG. PC is the most abundant mitochondrial phospholipid, but it is synthesized primarily in the ER (38). The involvement of MAMs in PC import

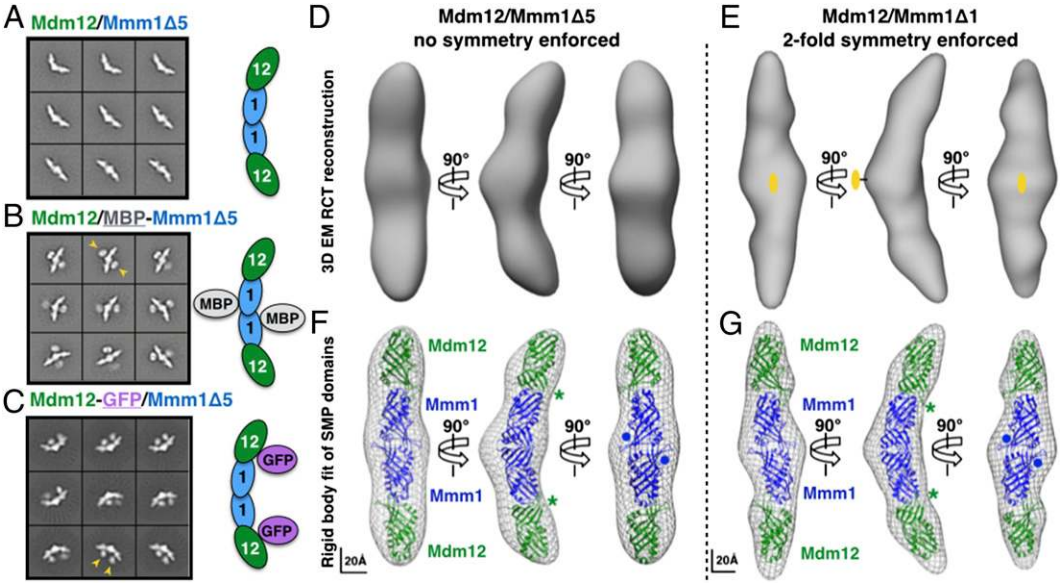

Fig. 7. Architecture of the Mdm12/Mmm1 subcomplex of the ERMES. Class averages obtained by negative-stain EM analysis and subunit positions: (*A*) Mdm12/Mmm1Δ5; (*B*) Mdm12/MBP-Mmm1Δ5; (*C*) Mdm12-GFP/Mmm1Δ5. Yellow arrowheads in *B* and *C* indicate additional electron-dense structures assigned to the GFP and MBP carrier proteins used to locate the Mdm12 and Mmm1Δ5 subunits, respectively. (*D* and *E*) Negative-stain EM 3D reconstructions of the Mdm12/Mmm1 heterotetramer. RCT reconstruction of the Mdm12/Mmm1Δ5 complex (35-Å resolution) (*D*) and RCT reconstruction of the Mdm12/Mmm1Δ1 complex (17-Å resolution) using untilted particle images and refined with twofold symmetry (*E*). (*F* and *G*) Modeling of four SMP domains by rigid body fitting of the E-SYT2 SMP domain crystal structure (PDB ID code 4P42) in the 3D electron-density maps. A central SMP dimer (blue) represents the Mmm1 homodimer and is decorated by two distal SMP domains corresponding to Mdm12 (green). The asterisks and dots indicate the positions of the C terminus of Mdm12 and N terminus of Mmm1, respectively; they agree with class averages shown in *A*–*C*. Scale bars are shown.

into mitochondria has not been established. Our findings demonstrate that PC might be the main physiological ligand of Mdm12 and Mmm1. Thus, it is attractive to hypothesize that ERMES facilitates this essential transport. The possibility that the observed lipid-binding preferences might change in the context of a fully assembled tether has not been completely dismissed.

These findings provide novel insights into the role of the SMP domain in the hierarchical assembly of the ERMES tether. Mdm12 was shown to play a central role in bridging the SMP domains of Mmm1 and Mdm34, providing a rationale for the previous observation that Mdm12 displays dual membrane localization. In the absence of Mdm34, Mdm12 is localized to the ER; however, in the absence of Mmm1, Mdm12 is localized to mitochondria (8). The interaction between Mdm12 and Mdm34 based on our pull-down assay is relatively weak compared with the interaction observed between Mdm12 and Mmm1. This result is not entirely unexpected for two possible reasons: (*i*) Because of the highly dynamic nature of the ER and mitochondria, a tightly associated tether might be physiologically unfavorable; (*ii*) it is conceivable that the regulatory subunit of ERMES, the Ca^{2+}-binding Miro GTPase Gem1, plays a regulatory role in modulating the binding interactions of the three ERMES subunits. In support of this hypothesis, Gem1 has been demonstrated to regulate ERMES organization directly, and its deletion alters the size and number of intracellular ERMES (10).

In addition to ERMES, other interorganelle-tethering complexes have been shown to consist of SMP-containing proteins. For example, tricalbins 1, 2, and 3, which are yeast homologs of the human E-SYTs, tether the ER and plasma membrane in yeast (39). Also, the nucleus-vacuole junction 2 protein (Nvj2p) is enriched at the nucleus–vacuole junction (18), and likely bridges the two organelles. Therefore it is attractive to speculate that the SMP domain might act as a general scaffold to facilitate protein–protein interactions that enable tether formation, resulting in the juxtaposition of organelles at MCS.

The 17-Å-resolution EM reconstruction of the Mdm12/Mmm1 complex revealed a 210-Å-long elongated, crescent-shaped assembly, in which a central Mmm1 dimer is flanked by two molecules of Mdm12 that project outwards. The dimer of Mmm1 is connected to its ER transmembrane anchor by a 50- to 70-residue-long flexible linker that could span a distance of 160 Å in a fully extended conformation (Fig. 8*A* and Fig. S9*A*). Homology models of the two proteins fitted into the EM density suggested the formation of an extended, tubular-shaped tunnel formed upon alignment of four SMP domains; each SMP harbors a hydrophobic interior for binding phospholipids. Based upon this information, we propose a comprehensive model of ERMES wherein the Mdm12/Mmm1 complex (which lies parallel to the plane of the ER membrane) associates with the dimerization-prone SMP domain of Mdm34 attached to the outer mitochondrial membrane (Fig. 8*A* and Fig. S9*A*). This arrangement places Mdm12 in a central bridging position (Fig. 4*C*). The flexible linkers that connect the SMPs of Mmm1 and Mdm34 to their respective membranes provide the necessary flexibility that can enable movement of the core assembly of the SMPs (Fig. 8*B*). In this organization, the interaction of all three proteins can easily accommodate the reported distance of ∼15–30 nm between organelles at MCS (40). However, the precise stoichiometry of a fully assembled tether remains unknown.

Currently, a mechanism for phospholipid exchange between the ER and mitochondria remains largely undefined. Given its location at ER–mitochondria junctions and the established role of its SMP domains in phospholipid binding, ERMES is very likely to facilitate such an exchange actively. Two examples of lipid transport systems that occur via nonvesicular mechanisms help explain how a complex such as ERMES could exchange lipids while, at the same time, tethering organelles. In the first example, the steroidogenic acute regulatory protein (STARD11) has been shown to tether the ER and Golgi apparatus via its Golgi membrane-associated pleckstrin homology domain and FFAT motif (two phenylalanines in an acidic tract) bound to the

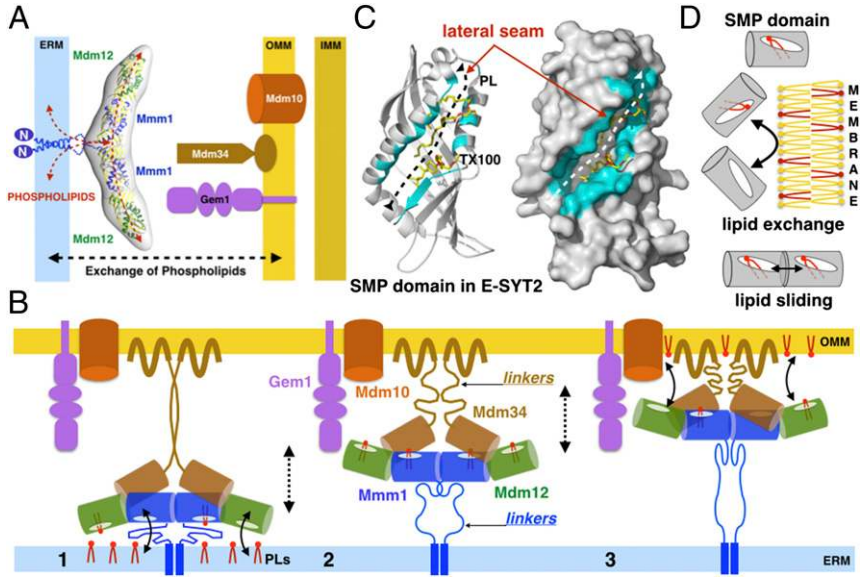

Fig. 8. ERMES and the exchange of phospholipids at ER–mitochondria membrane contact sites. (*A*) Structural and functional model of the ERMES Mdm12/Mmm1 subcomplex as a phospholipid transfer system at ER-to-mitochondria contact sites. (*B*) Model of ERMES accounting for the SMP-facilitated exchange of phospholipids. A ternary complex composed of all three SMPs diffuses back and forth between membranes to transport PLs. The long and flexible linkers on Mmm1 and Mdm34 tether the assembly to both membranes and enable movement. The SMP domains of Mdm12 and Mmm1 (and possibly Mdm34) extract phospholipids (PC and possibly others) from the ER membrane (1), and the complex diffuses between the two membranes (2) then delivers phospholipids to the outer mitochondria surface (3). This model is compatible with bidirectional exchange. Gem1 and Mdm10 subunits are depicted only on the side; the exact stoichiometry of the ternary assembly of SMPs is currently unknown. (*C*) A lateral opening in the SMP domain mediates phospholipid exchange and/or sliding. Ribbon and surface representations show the E-SYT2 SMP domain bound to a phospholipid and a Triton X-100 detergent molecule (TX100). Residues lining the lateral opening along the tubular TULIP fold are colored in cyan. (*D*) The SMP domains present in ERMES might act as phospholipid-extracting proteins capable of partitioning phospholipids in and out of membranes. Two aligned SMP domains also could exchange phospholipids by a sliding mechanism along their lateral openings.

ER vesicle-associated membrane-associated protein (VAP) (41, 42). This membrane-tethering arrangement has been shown to allow the lipid-binding START domain of STARD11 to transfer ceramide from the ER to Golgi in a swing-like mechanism. The second example involves the STARD3 protein that recently has been proposed to tether the ER and the late endosome and enable the exchange of cholesterol between the two organelles (43).

The crystal structure of E-SYT2 suggested two mechanisms of SMP-mediated phospholipid transport (23): (*i*) a tunnel model, wherein the elongated dimer of aligned SMP domains (Fig. 1*C*) bridges the two membranes and functions as a conduit to transport lipids; and (*ii*) a tethered shuttle model in which the SMP dimer shuttles between membranes, extracting lipids from one and delivering them to the other. The lateral opening along the side of the SMP β-barrel, a conserved feature of all TULIP proteins, might facilitate phospholipid transfer by maintaining the exposure of the polar head group to the solvent while nesting the fatty acid tails within the hydrophobic tunnel (Fig. 8*C*). Translocation systems that process diverse types of substrates such as nascent proteins (44, 45) and lipids (46) often use a lateral opening (referred to as the "lateral gate" or "seam") to partition their substrate between a proteinaceous binding pocket and a membrane. Such a system could facilitate the extraction and exchange of lipids from membranes or, in a more sophisticated model, the sliding of lipids from one SMP domain to another in the aligned configuration (Fig. 8*D*).

A model based on the tunnel model of E-SYT2 was proposed recently to explain how ERMES might facilitate lipid transport: Lang et al. (47) speculated that individual monomers of Mmm1 interact directly with Mdm34 or Mdm12 to form heterodimeric tunnels that run between the ER and mitochondria. However, our biochemical and structural data do not support the formation of such tunnels. Instead, we propose a model for transport in which the core Mmm1/Mdm12/Mdm34 assembly of SMPs partitions phospholipids from membranes and shuttles them back and forth between the ER and mitochondria (Fig. 8*B*). Diffusion is both controlled and facilitated by the flexible tethers on both membranes. In this aspect, our model is similar to the tethered shuttle elaborated by Schauder et al (23). This model is in contrast to oxysterol-binding homology protein 6 (Osh6), a different class of LTP that acts as a freely diffusible cytosolic shuttle capable of extracting PS from the ER and delivering it to the plasma membrane (48). Although the kinetics and detailed molecular mechanisms of lipid transport by ERMES remain to be elucidated, one possibility is that the net transfer of lipids likely depends on their concentration gradients. In this scenario, the enrichment of PC in the ER (the donor membrane), where it is synthesized, drives its transport to the primary site of use in mitochondria (the acceptor membrane). Indeed, the PC-transfer protein and the PI-transfer protein have been reported previously to facilitate lipid exchange in a similar fashion (49).

One feature that distinguishes the ERMES from E-SYT2 is that the ERMES requires multiple subunits to bridge two organelles (i.e., Mdm12 in the cytoplasm, Mmm1 on the ER, and Mdm34 on the mitochondrion), whereas E-SYT2 singly tethers ER and plasma membranes. Why would transfer of PC (or another phospholipid) require such elaborate machinery? The presence of proteins on both organelles could impart specificity, provide additional layers of regulation, and increase the efficiency of lipid transport. Future goals include the reconstitution of all five ERMES components to dissect rigorously the dynamic mechanisms that underlie membrane tethering and phospholipid exchange at ER–mitochondrial contact sites.

To the best of our knowledge, our work provides the first detailed biochemical and structural analyses of ERMES. Furthermore, the present combined data inform a model for how the SMP domains

of Mdm12, Mmm1, and Mdm34 assemble into a ternary complex with dual roles in membrane tethering and phospholipid exchange at ER–mitochondria contact sites. Our work provides the basis for understanding the structure and function of other SMP-containing tethering complexes at membrane contact sites.

Experimental Procedures

Detailed experimental procedures describing the modeling of Mdm12 and Mmm1 SMP domains, design of all expression constructs (for Mdm12, Mmm1, and Mdm34), protein expression in *E. coli* and *S. cerevisiae*, protein purification and characterization, Mdm12/Mmm1 complex reconstitution, lipid analyses by HPTLC and MS, characterization of the Mmm1/Mdm12/Mdm34 ternary complex by pull-down, and the structural analysis of the Mdm12/Mmm1 complex by EM are provided in *SI Experimental Procedures*.

ACKNOWLEDGMENTS. We thank Dan McNamara and Brendan Amer for help with the SEC-MALS experiments; Maxime Chapon, Anna Reichardt, Linda Yen, and Mark Arbing for thoughtful contributions to the manuscript; and Drs. James Wohlschlegel, Reid Johnson, and Greg Payne for suggestions regarding the manuscript. Lipid analyses were performed by Mary Roth at the Kansas Lipidomics Research Center Analytical Laboratory of Professor Ruth Welti. This work was supported by the University of California, Los Angeles (UCLA) Geffen School of Medicine; a Stein–Oppenheimer Endowment Award; National Center for Advancing Translational Sciences UCLA Clinical and Translational Science Institute Grant UL1TR000124; a Scholar in Translational Medicine Program Award; the Alexander and Renée Kolin Professorship in Molecular Biology and Biophysics (to P.F.E.); and National Institutes of Health Grants R01GM103479 and S10RR028893 (to J.A.L.). A.P.A. was supported by a Gates Millennium Fellowship and the Dissertation of the Year Fellowship. Instrument acquisition and lipidomics method development were supported by National Science Foundation Grants EPS 0236913, MCB 0920663, MCB 1413036, DBI 0521587, and DBI 1228622; Kansas Technology Enterprise Corporation; K-IDeA Networks of Biomedical Research Excellence of National Institute of Health Grant P20GM103418; and Kansas State University. We acknowledge the use of instruments and assistance at the Electron Imaging Center for NanoMachines supported by National Institutes of Health 1S10RR23057 and GM071940 (to Z.H.Z.) and the California NanoSystems Institute at UCLA.

1. Helle SC, et al. (2013) Organization and function of membrane contact sites. *Biochim Biophys Acta* 1833(11):2526–2541.
2. Elbaz Y, Schuldiner M (2011) Staying in touch: The molecular era of organelle contact sites. *Trends Biochem Sci* 36(11):616–623.
3. Tavassoli S, et al. (2013) Plasma membrane—endoplasmic reticulum contact sites regulate phosphatidylcholine synthesis. *EMBO Rep* 14(5):434–440.
4. Tatsuta T, Scharwey M, Langer T (2014) Mitochondrial lipid trafficking. *Trends Cell Biol* 24(1):44–52.
5. Tamura Y, Sesaki H, Endo T (2014) Phospholipid transport via mitochondria. *Traffic* 15(9):933–945.
6. Raturi A, Simmen T (2013) Where the endoplasmic reticulum and the mitochondrion tie the knot: The mitochondria-associated membrane (MAM). *Biochim Biophys Acta* 1833(1):213–224.
7. English AR, Voeltz GK (2013) Endoplasmic reticulum structure and interconnections with other organelles. *Cold Spring Harb Perspect Biol* 5(4):a013227.
8. Kornmann B, et al. (2009) An ER-mitochondria tethering complex revealed by a synthetic biology screen. *Science* 325(5939):477–481.
9. Stroud DA, et al. (2011) Composition and topology of the endoplasmic reticulum-mitochondria encounter structure. *J Mol Biol* 413(4):743–750.
10. Kornmann B, Osman C, Walter P (2011) The conserved GTPase Gem1 regulates endoplasmic reticulum-mitochondria connections. *Proc Natl Acad Sci USA* 108(34):14151–14156.
11. Nguyen TT, et al. (2012) Gem1 and ERMES do not directly affect phosphatidylserine transport from ER to mitochondria or mitochondrial inheritance. *Traffic* 13(6):880–890.
12. Voss C, Lahiri S, Young BP, Loewen CJ, Prinz WA (2012) ER-shaping proteins facilitate lipid exchange between the ER and mitochondria in S. cerevisiae. *J Cell Sci* 125(Pt 20):4791–4799.
13. Hönscher C, et al. (2014) Cellular metabolism regulates contact sites between vacuoles and mitochondria. *Dev Cell* 30(1):86–94.
14. Elbaz-Alon Y, et al. (2014) A dynamic interface between vacuoles and mitochondria in yeast. *Dev Cell* 30(1):95–102.
15. Lee I, Hong W (2006) Diverse membrane-associated proteins contain a novel SMP domain. *FASEB J* 20(2):202–206.
16. Kopec KO, Alva V, Lupas AN (2010) Homology of SMP domains to the TULIP superfamily of lipid-binding proteins provides a structural basis for lipid exchange between ER and mitochondria. *Bioinformatics* 26(16):1927–1931.
17. Kopec KO, Alva V, Lupas AN (2011) Bioinformatics of the TULIP domain superfamily. *Biochem Soc Trans* 39(4):1033–1038.
18. Toulmay A, Prinz WA (2012) A conserved membrane-binding domain targets proteins to organelle contact sites. *J Cell Sci* 125(Pt 1):49–58.
19. Hamiaux C, Stanley D, Greenwood DR, Baker EN, Newcomb RD (2009) Crystal structure of Epiphyas postvittana takeout 1 with bound ubiquinone supports a role as ligand carriers for takeout proteins in insects. *J Biol Chem* 284(6):3496–3503.
20. Beamer LJ, Carroll SF, Eisenberg D (1997) Crystal structure of human BPI and two bound phospholipids at 2.4 angstrom resolution. *Science* 276(5320):1861–1864.
21. Qiu X, et al. (2007) Crystal structure of cholesteryl ester transfer protein reveals a long tunnel and four bound lipid molecules. *Nat Struct Mol Biol* 14(2):106–113.
22. Eckert JK, et al. (2013) The crystal structure of lipopolysaccharide binding protein reveals the location of a frequent mutation that impairs innate immunity. *Immunity* 39(4):647–660.
23. Schauder CM, et al. (2014) Structure of a lipid-bound extended synaptotagmin indicates a role in lipid transfer. *Nature* 510(7506):552–555.
24. Kelley LA, Sternberg MJ (2009) Protein structure prediction on the Web: A case study using the Phyre server. *Nat Protoc* 4(3):363–371.
25. Wideman JG, Gawryluk RMR, Gray MW, Dacks JB (2013) The ancient and widespread nature of the ER-mitochondria encounter structure. *Mol Biol Evol* 30(9):2044–2049.
26. Glaser F, et al. (2003) ConSurf: Identification of functional regions in proteins by surface-mapping of phylogenetic information. *Bioinformatics* 19(1):163–164.
27. Flinner N, et al. (2013) Mdm10 is an ancient eukaryotic porin co-occurring with the ERMES complex. *Biochim Biophys Acta* 1833(12):3314–3325.
28. Ghaemmaghami S, et al. (2003) Global analysis of protein expression in yeast. *Nature* 425(6959):737–741.
29. Sohlenkamp C, López-Lara IM, Geiger O (2003) Biosynthesis of phosphatidylcholine in bacteria. *Prog Lipid Res* 42(2):115–162.
30. Horvath SE, Daum G (2013) Lipids of mitochondria. *Prog Lipid Res* 52(4):590–614.
31. Daum G, Vance JE (1997) Import of lipids into mitochondria. *Prog Lipid Res* 36(2-3):103–130.
32. Daum G, et al. (1999) Systematic analysis of yeast strains with possible defects in lipid metabolism. *Yeast* 15(7):601–614.
33. Ejsing CS, et al. (2009) Global analysis of the yeast lipidome by quantitative shotgun mass spectrometry. *Proc Natl Acad Sci USA* 106(7):2136–2141.
34. van Meer G, Voelker DR, Feigenson GW (2008) Membrane lipids: Where they are and how they behave. *Nat Rev Mol Cell Biol* 9(2):112–124.
35. Radermacher M, Wagenknecht T, Verschoor A, Frank J (1987) Three-dimensional reconstruction from a single-exposure, random conical tilt series applied to the 50S ribosomal subunit of Escherichia coli. *J Microsc* 146(Pt 2):113–136.
36. Beamer LJ, Carroll SF, Eisenberg D (1998) The BPI/LBP family of proteins: A structural analysis of conserved regions. *Protein Sci* 7(4):906–914.
37. Toulmay A, Prinz WA (2011) Lipid transfer and signaling at organelle contact sites: The tip of the iceberg. *Curr Opin Cell Biol* 23(4):458–463.
38. Vance JE (2014) MAM (mitochondria-associated membranes) in mammalian cells: Lipids and beyond. *Biochim Biophys Acta* 1841(4):595–609.
39. Manford AG, Stefan CJ, Yuan HL, Macgurn JA, Emr SD (2012) ER-to-plasma membrane tethering proteins regulate cell signaling and ER morphology. *Dev Cell* 23(6):1129–1140.
40. Csordás G, et al. (2010) Imaging interorganelle contacts and local calcium dynamics at the ER-mitochondrial interface. *Mol Cell* 39(1):121–132.
41. Hanada K, et al. (2003) Molecular machinery for non-vesicular trafficking of ceramide. *Nature* 426(6968):803–809.
42. Hanada K, Kumagai K, Tomishige N, Yamaji T (2009) CERT-mediated trafficking of ceramide. *Biochim Biophys Acta* 1791(7):684–691.
43. Alpy F, Tomasetto C (2014) START ships lipids across interorganelle space. *Biochimie* 96:85–95.
44. Egea PF, Stroud RM (2010) Lateral opening of a translocon upon entry of protein suggests the mechanism of insertion into membranes. *Proc Natl Acad Sci USA* 107(40):17182–17187.
45. Noinaj N, et al. (2013) Structural insight into the biogenesis of β-barrel membrane proteins. *Nature* 501(7467):385–390.
46. Hearn EM, Patel DR, Lepore BW, Indic M, van den Berg B (2009) Transmembrane passage of hydrophobic compounds through a protein channel wall. *Nature* 458(7236):367–370.
47. Lang A, John Peter AT, Kornmann B (2015) ER-mitochondria contact sites in yeast: Beyond the myths of ERMES. *Curr Opin Cell Biol* 35:7–12.
48. Maeda K, et al. (2013) Interactome map uncovers phosphatidylserine transport by oxysterol-binding proteins. *Nature* 501(7466):257–261.
49. Lev S (2010) Non-vesicular lipid transport by lipid-transfer proteins and beyond. *Nat Rev Mol Cell Biol* 11(10):739–750.

Supporting Information

AhYoung et al. 10.1073/pnas.1422363112

SI Experimental Procedures

Homology Modeling in Phyre[2]. Mdm12 and Mmm1 SMP domains were modeled in Phyre[2]. The quality of the corresponding models is evaluated using the confidence and percentage of sequence identity estimated for each template PDB structure used to model the target protein. For confidence greater than 90%, one generally can be very confident that the query protein adopts the overall fold shown and that the core of the protein is modeled at high accuracy (2- to 4-Å rmsd from the native, true structure). However, surface loops probably will deviate from the native structure. The percentage of sequence identity between the target sequence and the PDB template determines the likely accuracy of the model. For extremely high-accuracy models, numbers should be above 30–40%. However, even at very low sequence identities (<15%) models can be meaningful and useful as long as the confidence is high. Results are summarized in Fig. S3*B*.

Sequence Conservation Analysis. The Mdm12 and Mmm1 sequences of 26 organisms (21 fungi, four amoebas, and one filasterian) were retrieved and aligned in PSI-Blast; the resulting alignments were used to estimate the sequence conservation scores with ConSurf.

***Yeasts and fungi*.** The yeasts and fungi used were *S. cerevisiae*, *S. castellii*, *Schizosaccharomyces pombe*, *Schizosaccharomyces japonicus*, *Candida albicans*, *Neurospora crassa*, *Aspergillus fumigatus*, *Yarrowia lipolytica*, *Ustilago maydis*, *Cryptococcus neoformans*, *Scheffersomyces stipitis*, *Millerozyma farinosa*, *Serpula lacrymans*, *Melanspora larici-populina*, *Rhizopus oryzae*, *Dichomitus squalens*, *Tuber melanosporum*, *Leptosphaeria maculans*, *Batrachochytrium dendrobatidis*, *Pyromyces* sp., and *Dacryopinax* sp.

***Amoebas*.** The amoebas used were *D. discoideum*, *Dictyostelium fasciculatum*, *Dictyostelium purpureum*, and *Naegleria gruberi*.

***Filasterians*.** The filasterian used, *Capsaspora owczarzaski*, is one of the closest unicellular relatives of multicellular organisms (1).

Protein and Complex Expression Construct Designs. The *S. cerevisiae* (*Sce*) Mdm12, Mmm1, and Mdm34 genes and the *S. castellii* (*Scas*) Mdm12 gene were cloned by PCR using total genomic DNAs. The *D. discoideum* (*Ddis*) Mdm12 gene was synthetized after codon optimization for its expression in *E. coli* (DNA2.0 Inc.). Fig. S2*C* summarizes all constructs used in this study.

***Mdm12 expression constructs in* E. coli.** *Sce*-Mdm12 constructs were cloned into a pCDF (streptomycin resistance) expression vector (Novagen). All constructs of *Sce*-Mmm1 were cloned into a pRSF (kanamycin resistance) expression vector (Novagen). For *Sce*-Mdm12, the single point mutant C92S also was introduced to improve the homogeneity of the purified protein and reduce disulfide bond-mediated oligomerization. *Scas*-Mdm12 and *Ddis*-Mdm12 proteins were cloned into a pRSF vector to be expressed as fusion proteins with a His-tagged MBP carrier protein at the N terminus and an additional His tag at the C terminus of the Mdm12 protein. A thrombin cleavage site was present to sever the His-MBP carrier and the C-terminal His tag from the Mdm12 protein of interest. For *Sce*-Mdm12, we also constructed a pRSF vector to express *Sce*-Mdm12 fused to a superfolder GFP at its C terminus followed by a His tag (sfGFP-His). In this case the sfGFP carrier cannot be severed from Mdm12, but the His tag that follows can; this construct was used for crystallization trials and electron microscopy.

***Mmm1 expression constructs in* E. coli.** Eight deletion constructs mapping to the cytoplasmic domain of *Sce*-Mmm1 were generated through systematic deletion by 10-residue increments starting at the N terminus of the predicted cytoplasmic domain of *Sce*-Mmm1. These different constructs were cloned in a pRSF vector with an N-terminal MBP carrier protein and a C-terminal His tag. Construct Mmm1Δ1 (residues 122–426) encompasses the entire cytoplasmic domain. Construct Mmm1Δ5 (residues 181–426) encompasses the SMP domain that was modeled in Phyre[2] and used for most of the biochemical and structural work. Construct Mmm1Δ7 (residues 201–426) encompasses the SMP domain *stricto senso*. Residues 1–100 and 101–121 correspond to the short glycosylated luminal domain and the single transmembrane-spanning helix, respectively (Fig. S2*A*).

***Mdm34 expression constructs in* E. coli.** Three deletion constructs mapping to the predicted cytoplasmic SMP domain of *Sce*-Mdm34 were generated starting at the N terminus. These different constructs were cloned in a pGEX-4T1 (ampicillin resistance) vector with an N-terminal GST carrier protein and a C-terminal His tag. The same constructs were cloned in a pRSF vector with an N-terminal GFP fusion protein and a C-terminal His tag. Construct Mdm34 SMP1 (residues 1–188) encompasses the SMP domain and was used for biochemical characterization (characterization on its own and in association with Mdm12 and Mmm1 by pull-down) and lipid analysis (Fig. S2*B*). A specific construct was generated consisting of GST fused to Mdm34 SMP1-His with a tobacco etch virus (TEV) protease cleavage site introduced between GST and the SMP, and the protein was cleaved in vivo by coexpressing the GST-tev-Mdm34 SMP-His protein with a plasmid producing TEV protease (2). The Mdm34 SMP domain was severed from its GST partner by TEV protease in vivo and purified using the His tag.

***Constructs for Mdm12/Mmm1 coexpression and copurification*.** Mdm12/Mmm1 complexes were coexpressed by cotransformation of two vectors in the same cells, because the alternative strategy based on the use of a single plasmid containing both Mdm12 and Mmm1 genes proved less effective. Preliminary expression tests indicated that coexpression was limited by the amount of Mmm1 efficiently produced in *E. coli*, whereas Mdm12 appeared to be in large excess. Thus the Mdm12 protein was expressed with a C-terminal Flag peptide tag, and the different Mmm1 constructs were expressed as MBP-fusion proteins carrying a C-terminal His tag (Fig. S2*C*).

***Bacterial heterologous expression*.** Expression and purification of the abovementioned proteins were performed using the following protocol. *E. coli* C43 (DE3) cells were transformed with one or two plasmids for single or coexpression tests, respectively. Freshly transformed cells were used to inoculate an overnight preculture of LB broth medium at 37 °C. The next day, 3–6 L of LB were inoculated with preculture and grown at 37 °C to an optical density at 600 nm of 0.5–0.8, at which point the temperature was lowered to 20 °C for 1 h. Protein expression then was induced by adding isopropyl-β-D-thiogalactoside (IPTG) at 0.8 mM final concentration. After 5 h of culture, cells were pelleted, washed in 150 mM KCl and 20 mM Tris (pH 7.8), and stored at −80 °C until processing.

***Yeast homologous expression*.** Yeast Mdm12 was overexpressed in yeast using a pY23GAL10-GPD bidirectional expression plasmid (3) with the yeast Mdm12 gene placed under the control of the constitutive GPD promoter. The protein was cloned with a C-terminal noncleavable octa-His tag. Cells were transformed and plated on complete synthetic complete with glucose-HIS (CSMG-HIS) selective medium. A 9-L culture of yeast in CSMG-HIS was grown at 28 °C for 24 h. Cells were pelleted, washed in 150 mM KCl and 20 mM Tris (pH 7.8), and stored at −80 °C until processing.

Protein and Complex Purification.

***ERMES proteins and Mdm12/Mmm1 complexes expressed in* E. coli *(heterologous expression)*.** Thawed cell pellets were resuspended in lysis buffer [500 mM NaCl, 20 mM Tris (pH 7.8), 15% glycerol] supplemented with 2.8 mM β-mercaptoethanol (βme), 0.2 mM of PMSF, and one tablet of EDTA-free protease inhibitor mixture (Roche). All subsequent steps were carried out at 4 °C or on ice. Cells were lysed by three passes through a C-3 Emulsiflex (Avestin) pressurized at 14,000 psi. The lysate was clarified by centrifugation at 25,000 × *g* for 1 h, after which the resulting supernatant corresponding to the total soluble extract was applied onto a gravity-flow column (Bio-Rad) packed with 5–10 mL of cobalt-NTA immobilized metal affinity chromatography (IMAC) resin (Thermo Fisher). Nonspecifically bound bacterial proteins were washed from the column using Cobalt-A wash buffer [12.5 mM imidazole, 500 mM NaCl, 20 mM Tris (pH 7.8), 10% glycerol, 1.4 mM βme, and 0.2 mM PMSF]. The protein or complex of interest (purified on the basis of an N- or/and C-terminal His tag) was eluted from the column with Cobalt-B buffer [125 mM imidazole, 500 mM NaCl, 20 mM Tris (pH 7.8), 10% glycerol, 1.4 mM βme, and 0.2 mM PMSF]. The IMAC eluate was concentrated to 0.5–1 mL using a 10-, 30-, or 50-kDa cutoff Centricon (EMD Millipore) centrifugal filter, depending on the molecular weight of the protein and was desalted using a PD-10 desalting column (Bio-Rad) equilibrated in 100 mM NaCl, 20 mM Tris (pH 7.8), 2% glycerol, 1.4 mM βme, and 0.2 mM PMSF to remove imidazole. After desalting, the protein or complex of interest was purified by anion exchange chromatography (aIEX) on CaptoQ HiTrap columns (GE Healthcare). Unless otherwise specified, the sample was treated with thrombin for 24 h at 4 °C (0.25 units enzyme/mg protein) to remove His and/or Flag-peptide purification tags and/or the MBP or superfolder GFP carrier proteins when applicable. After thrombin treatment, the sample was purified further on a mixture of Ni-NTA IMAC (Thermo Fisher) and Benzamidine-Sepharose (GE Healthcare) to subtract unprocessed tagged protein, tags, and thrombin simultaneously. The final purification step consisted of SEC on a Superdex 200 HR10/30 column (GE Healthcare) equilibrated in 100 mM NaCl, 20 mM Tris (pH 7.8), 2% glycerol, and 0.15 mM Tris(2-carboxyethyl)phosphine (TCEP). For GST-Mdm34 SMP (purified with its GST still attached), lysis was performed in the same buffer, but after purification of the GST-Mdm34 SMP-His proteins on cobalt-NTA IMAC resin, the eluate was loaded on a HiCap GST column (Qiagen) equilibrated in 300 mM NaCl, 2% glycerol, 50 mM Tris (pH 7.8), 0.5 mM EDTA, and 2 mM DTT. After washing, the GST fusion was eluted using the same buffer supplemented with reduced glutathione at 50 mM. After elution, the excess glutathione was removed either by dialysis or by desalting. The protein was purified further by SEC on a Superdex 200 HR10/30 column equilibrated in 300 mM NaCl, 20 mM Tris (pH 7.8), 2% glycerol, and 0.15 mM TCEP. Mdm34 SMP-His protein generated by intracellular TEV cleavage was purified by cobalt-NTA IMAC and SEC. The purity of samples generated for every experiment was assessed by SDS/PAGE stained with Coomassie blue.

***Yeast Mdm12 expressed in yeast (homologous expression)*.** Thawed cell pellets from a 9-L culture were resuspended in lysis buffer [500 mM NaCl, 40 mM Tris (pH 7.8), 15% glycerol] supplemented with 7 mM βme, 0.1 mM TCEP, 0.2 mM PMSF, and two tablets of EDTA-free protease inhibitor mixture (Roche). Then 225 mL of autoclaved glass beads (0.5-mm diameter) were added to 225 mL of the cell suspension. All subsequent steps were carried out at 4 °C. Cells were disrupted using a bead beater (BioSpec) (four cycles: 45 s of homogenization followed by 2.25 min of recovery to minimize sample heating). Beads were decanted, and the lysate was clarified by centrifugation at 25,000 × *g* for 1.5 h, after which the resulting supernatant corresponding to the total soluble extract was incubated with 15 mL cobalt-NTA IMAC resin (Qiagen) for batch binding for 1 h. Nonspecifically bound yeast proteins were washed from the column using Nickel-A wash buffer [25 mM imidazole, 500 mM NaCl, 20 mM Tris (pH 7.8), 10% glycerol, 7 mM βme, and 0.2 mM PMSF]. *Sce*-Mdm12 was eluted from the column with Nickel-B buffer [250 mM imidazole, 500 mM NaCl, 20 mM Tris (pH 7.8), 10% glycerol, 7 mM βme, and 0.2 mM PMSF]. Yeast Mdm12 was purified by aIEX on CaptoQ HiTrap columns (GE Healthcare). The protein was repurified using a 1-mL Ni-HiTrap column (GE Healthcare). A final SEC purification step was performed on a Superdex 200 HR 10/30 column equilibrated in 300 mM NaCl, 20 mM Tris (pH 7.6), 2% glycerol, and 0.1 mM TCEP.

***SEC-MALS to determine absolute mass of proteins*.** To characterize Mdm12, Mdm12/Mmm1Δ5, and Mdm12/MBP-Mmm1Δ5 by SEC-MALS, the proteins were gel-filtrated into 20 mM Tris (pH 7.8), 200 mM NaCl, 2% glycerol, and 14 mM βme. The peak fraction for each gel filtration was used for SEC-MALS. An analytical SEC column (5 μm, 300 Å, 7.8 × 300 mm; Wyatt Technology) was equilibrated in 20 mM Tris, 200 mM NaCl, 2% glycerol, and 14 mM βme. In each case, a 100-μL sample (50 μM Mdm12, 20 μM Mdm12/Mmm1Δ5, or 14 μM Mdm12/MBP-Mmm1Δ5) was injected. The smaller the size of the protein, the more protein was needed to detect light-scattering signals. During elution, light scattering was measured with a miniDAWN TREOS (Wyatt Technology), and the refractive index (*n*) was measured with an Optilab T-rEX system (Wyatt Technology). The data were analyzed by ASTRA 6 software to obtain average molecular weights (Figs. 3 *D–F* and 4). The *dn*/*dc* (where *c* is concentration) for the calculation was set to 0.185 mL/g, a typical value for proteins.

***Pull-down analysis of protein–protein interactions between SMP domains in ERMES*.** To test for interactions between SMP domains of ERMES, 100 μL of purified His-tagged Mdm34-SMP-His at 70 μM was prebound to 100 μL of cobalt-NTA IMAC resin suspension, washed, and equilibrated with binding buffer [150 mM NaCl, 20 mM Tris (pH 7.5), 2% glycerol, and 0.1 mM TCEP]. The prebinding reaction was incubated at 4 °C with gentle shaking for 30 min, after which the column was centrifuged at 100 × *g* for 3 min to remove unbound bait protein and excess buffer. The resin then was washed with 500 μL of binding buffer and spun for another 3 min. Next, 100 μL of untagged prey protein—purified Mdm12 (150 μM), Mmm1Δ5 (150 μM), or Mdm12/Mmm1Δ5 complex (300 μM)—was added, and each reaction was incubated at 4 °C with gentle shaking for 30 min. Reactions were centrifuged for 3 min at 100 × *g* and washed three times with 350 μL of wash buffer [12.5 mM imidazole, 150 mM NaCl, 20 mM Tris (pH 7.5), and 2% glycerol]. Proteins then were eluted with 100 μL of elution buffer [500 mM imidazole, 150 mM NaCl, 20 mM Tris (pH 7.5), and 2% glycerol]. To control for nonspecific binding, prey proteins were incubated with resin in the absence of the bait protein Mdm34-SMP-His and were processed similarly. Equivalent amounts of each reaction were loaded on SDS/PAGE revealed by silver staining.

Lipid Analyses.

***Lipid identification by HPTLC*.** To characterize endogenous ligands/phospholipids bound to Mdm12, the SMP domain of Mmm1 (Mmm1Δ5 and Mmm1Δ1), and the Mdm12/Mmm1Δ5 and Mdm12/Mmm1Δ1 complexes, lipids from these purified proteins were extracted and analyzed by HPTLC. Lipids were extracted as previously described (4) using the method of Bligh and Dyer (5). Briefly, we extracted lipids from 50 μL of purified protein or complex (~10 mg/mL or ~0.3 mM) by the sequential addition of 3.75 volumes of chloroform:methanol (1:2 vol/vol), 1.25 volumes of chloroform, and 1.25 volumes of 0.5% acetic acid in 500 mM NaCl followed by 1 min of vortexing after each step. The sample was centrifuged at maximum speed (14,000 × *g*) using a tabletop centrifuge for 15 min; then the bottom layer was gently recovered

and lyophilized. The resulting material was dissolved in 30 μL of methanol and loaded onto a silica gel 60 HPTLC plate (10 × 10 cm) (Merck). Plates were developed sequentially, first with a phase composed of dichloromethane:ethyl-acetate:acetone (80:16:4) and then with a phase composed of chloroform:acetone:isopropanol: ethyl-acetate:ethanol:methanol:water: acetic acid (30:6:6:6:16:28:6:2) (6). The plates were vacuum-dried, dripped in a 10% (wt/vol) $CuSO_4$ solution in 8% (vol/vol) aqueous phosphoric acid, and charred at 145 °C for 4.5 min (7).

In vitro lipid displacement assay. His-tagged Mdm12 (Mdm12-His_6) purified from *E. coli* was incubated with a twofold molar excess of the fluorescent phospholipid NBD-PE (Avanti Polar Lipids) for 2 h on ice. To remove excess unbound NBD-PE, Mdm12-His_6 was bound to an Ni-NTA spin column (Qiagen) and washed twice with ∼500 μL of wash buffer [25 mM imidazole (pH 7.5), 10 mM Hepes (pH 7.5), and 250 mM NaCl]. The Mdm12-His_6/NBD-PE complex was eluted with 200 μL of elution buffer [250 mM imidazole (pH 7.5), 250 mM NaCl, 10 mM Hepes (pH 7.5)] and further dialyzed against 1 L of buffer [250 mM NaCl and 10 mM Hepes (pH 7.5)] for 1 h at 4 °C using a 10,000 molecular weight cut-off (MWCO) Slide-A-Lyzer dialysis cassette (Thermo Scientific). Mdm12-His_6 was quantified and concentrated to a final concentration of ∼1.7 mg/mL for the lipid-binding and competition assay. NBD-PE binding to Mdm12 was assessed by BN-PAGE followed by Coomassie staining and fluorescence detection (extinction/emission, 460 nm/535 nm) for quantification using an ImageQuant LAS4000 molecular imager (GE Healthcare).

In a 20-μL reaction, Mdm12-His_6 preloaded with NBD-PE (10 μL at ∼1.7 mg/mL) was mixed with 9 μL of buffer [250 mM NaCl and 10 mM Hepes (pH 7.5)] and 1 μL of 10-mM competitor phospholipid resuspended in methanol. The final protein:lipid concentration ratio in the reaction is 0.028 mM:0.5 mM (∼18-fold excess of phospholipid). A lipid-only control (19 μL of buffer and 1 μL NBD-PE 10 mM stock) and protein-only control (10 μL of Mdm12-His_6 preloaded with NBD-PE at ∼1.7 mg/mL incubated with 1 μL of methanol plus 9 μL of buffer) also were included in the assay. The reactions were incubated on ice for 1 h and analyzed by BN-PAGE followed by Coomassie staining and fluorescence detection (extinction/emission 460 nm/535 nm) for quantification using an ImageQuant LAS4000 bimolecular imager. Each experiment was performed in triplicate.

All solvents used for HPTLC were purchased from Merck (HPLC grade). Phospholipids used as HPTLC standards and in the competition assay were purchased from Avanti Polar Lipids: *E. coli* (bacterial) total lipid extract, *S. cerevisiae* (yeast) total lipid extract, 1,2-dioleoyl-*sn*-glycero-3-phospho-L-serine (PS), 1,2-dioleoyl-*sn*-glycero-3-phosphoethanolamine (PE), 1,2-dioleoyl-*sn*-glycero-3-phosphocholine (PC), L-α-phosphatidic acid (PA), *E. coli* L-α-phosphatidylglycerol (PG), *E. coli* cardiolipin (CL), and L-α-phosphatidylinositol (PI). The lipids were dried under nitrogen and resuspended in methanol at a final concentration of 10 mM. The resulting displacements are shown in Fig. S7*D*.

In vitro lipid displacement assay in the presence of detergent. NBD-PE preloaded Mdm12-His_6 was prepared as described above before being incubated with six distinct detergents present at twice their critical CMC: Triton X-100 [TX100, CMC = 0.01% (wt/vol) = 0.15 mM]; n-Dodecyl β-d-maltoside (DDM; CMC = 0.12 mM); CHAPS (CMC = 8 mM); LDAO (CMC = 0.14 mM); foscholine-14 (FC14; CMC = 0.12 mM); and LFC10 (CMC = 3.2 mM) to quantify the effect of detergent on the binding of the fluorescent lipid. The reactions were incubated on ice for 1 h and analyzed by BN-PAGE followed by Coomassie staining and fluorescence detection for quantification (Fig. S7*A*). Mdm12-His_6 preloading with NBD-PE also was performed in the presence of the same six distinct detergents present at twice their respective CMCs to quantify the effect of detergent on fluorescent lipid preloading. After loading in presence of detergent, excess unbound NBD-PE was removed by dialysis, and reactions were analyzed by BN-PAGE followed by Coomassie staining and fluorescence detection for quantification (Fig. S7*B*). All detergents were purchased from Anatrace, and the reported CMCs are referenced or determined by Anatrace (Fig. S7*C*). LDAO was the best candidate detergent: It enhanced NBD-PE preloading 2.7-fold (Fig. S7*A*) but did not displace it (<10% loss) (Fig. S7*B*); thus it facilitates binding but does not displace NBD-PE. For the final lipid displacement reported in Fig. 5*C*, Mdm12-His was preloaded with NBD-PE in presence of LDAO (0.2 mM, 2× CMC) and then was incubated in the presence of the specific competitor phospholipids solubilized in the presence of LDAO (0.2 mM, 2× CMC) to measure displacement.

In vitro lipid transfer assay from liposomes. Yeast total lipid extract (7.5 mg) or yeast total polar lipid extract (5 mg) dissolved in chloroform was gently dried under a stream of N_2. The resulting lipid film was hydrated with 800 μL of 200 mM NaCl, 20 mM Tris (pH 7.5) and filtered to 400-nm liposomes using an extruder (Avanti Polar Lipids) to reach total lipid concentrations of ∼9.4 mg/mL (equivalent to ∼2.3 mM PC) and ∼6.25 mg/mL (equivalent to ∼2.4 mM PC), respectively. For lipid transfer experiments, the pure His-tagged Mdm12, MBP-Mmm1Δ5, or Mdm12/Mmm1Δ5 complex was concentrated to 0.5 mM, 0.5 mM, or 0.125 mM, respectively. Then 75 μL of each was incubated with 75 μL of either yeast total lipid or yeast total polar lipid liposomes. The reactions were incubated at room temperature for 1 h to enable lipid exchange and transfer from the liposome to the protein. Proteins then were purified on Ni-NTA spin columns (Thermo Fisher). The bound proteins were washed extensively (3 × 500 μL) with wash buffer [25 mM imidazole, 20 mM Tris (pH 7.5), and 300 mM NaCl] to remove unbound lipids and liposomes and were eluted with 400 μL elution buffer [500 mM imidazole, 20 mM Tris (pH 7.5), and 300 mM NaCl]. The resulting eluate was subjected to a Bligh and Dyer (5) extraction as previously described. The organic phase (bottom layer) was recovered and analyzed by HPTLC. Similarly, a liposome background control consisting of an identical amount of liposomes incubated with buffer but no protein also was subjected to Ni-NTA purification and lipid extraction before HPTLC analysis; under these conditions, no liposome carryover was observed in the final eluate (Fig. 6*C*).

BN-PAGE and clear native PAGE. BN-PAGE was performed using Bis-Tris 4–16% acrylamide gradient gels (Invitrogen Life Sciences). The anode (lower) buffer system was 50 mM BisTris/50 mM Tricine at pH 6.8. The cathode (upper) buffer system was 50 mM Bis-Tris/50 mM Tricine at pH 6.8 with 0.002% Coomassie G-250 blue dye. For clear native PAGE (CN-PAGE), no Coomassie G-250 blue dye was added in the cathode buffer. Gels were run first at 150 V for 60 min and then at 250 V for 50 min at 4 °C. Mdm12 was analyzed by BN-PAGE; MBP-Mmm1Δ5 and Mdm12/Mmm1Δ5 were analyzed by CN-PAGE.

MS Analyses.

Native MS. Purified protein samples were further desalted with a Vivaspin 10,000 MWCO centrifugal filter device (GE Healthcare) to exchange the initial buffer with 20 mM ammonium acetate at pH 6.8 and to eliminate eventual contaminating small molecules and minimize the amount of protein–salt adducts. Native MS experiments were performed on a 15-T Bruker SolariX Fourier transform ion cyclotron resonance (FTICR) mass spectrometer and a Waters SynaptG1 quadrupole TOF (QTOF) mass spectrometer. Briefly, the protein samples were prepared in 20–50 mM NH_4OAc solutions at a final concentration of 20 μM. The protein solutions were loaded into a nano-ESI source with Au/Pd coating on a borosilicate emitter (Thermo Scientific) and were electro-sprayed at 1–1.2 kV with a flow rate of 30–50 nL/min. The capillary temperature was set at 120 °C. For Fourier transform

(FT)-MS, the estimated resolving power was 400,000 at 400 *m/z*. FT-MS data were processed with DataAnalysis (Bruker Daltonics) and BioTools software and were annotated manually for accurate ion assignment. QTOF data were processed using MassLynx software and deconvoluted with MaxEnt1.

ESI-MS/MS quantitative lipid profiling. An automated ESI-MS/MS approach was used, and data acquisition and analysis were carried out as described previously (8), with modifications. The lipid samples were dissolved in 1 mL chloroform. An aliquot of 15–150 μL of extract in chloroform was used. Precise amounts of internal standards, obtained and quantified as previously described (9), were added in the following quantities (with some small variations in amounts in different batches of internal standards): 0.3 nmol di12:0-PC, 0.3 nmol di24:1-PC, 0.3 nmol 13:0-lysoPC, 0.3 nmol 19:0-lysoPC, 0.3 nmol di12:0-PE, 0.3 nmol di23:0-PE, 0.3 nmol 14:0-lysoPE, 0.3 nmol 18:0-lysoPE, 0.3 nmol di14:0-PG, 0.3 nmol di20:0 (phytanoyl)-PG, 0.3 nmol di14:0-PA, 0.3 nmol di20:0(phytanoyl)-PA, 0.2 nmol di14:0-PS, 0.2 nmol di20:0(phytanoyl)-PS, 0.46 nmol 16:0–18:0-PI, 0.33 nmol di18:0-PI. The sample and internal standard mixture was combined with solvents so that the ratio of chloroform:methanol:300 mM ammonium acetate in water was 300:665:35, and the final volume was 1.4 mL.

Unfractionated lipid extracts were introduced by continuous infusion into the ESI source on a triple quadrupole MS (4000QTrap; Applied Biosystems). Samples were introduced using an autosampler (LC Mini PAL; CTC Analytics AG) fitted with the required injection loop for the acquisition time and presented to the ESI needle at 30 μL/min. Sequential precursor and neutral loss scans of the extracts produce a series of spectra with each spectrum revealing a set of lipid species containing a common head group fragment. Lipid species were detected with the following scans for samples isolated from bacteria: PE and lysoPE, $[M + H]^+$ ions in positive ion mode with neutral loss of 141.0 (NL 141.0); PG, $[M + NH_4]^+$ in positive ion mode with NL 189.0. For samples isolated from yeast, scans were PC and lysoPC, $[M + H]^+$ ions in positive ion mode with precursor of 184.1 (Pre 184.1); PE and lysoPE, $[M + H]^+$ ions in positive ion mode with NL 141.0; PG, $[M + NH_4]^+$ in positive ion mode with NL 189.0; PI, $[M + NH_4]^+$ in positive ion mode with NL 277.0; PS, $[M + H]^+$ in positive ion mode with NL 185.0. The collision gas pressure was set at 2 (arbitrary units). The collision energies, with nitrogen in the collision cell, were +28 V for PE (and lysoPE); +40 V for PC (and lysoPC), PI, and PS; and +20 V for PG. Declustering potentials were +100 V for all positive-mode scans. Entrance potentials were +15 V for PE and +14 V for PC, PG, PI, and PS. Exit potentials were +11 V for PE and +14 V for PC, PG, PI, and PS. The scan speed was 50 or 100 u/s. The mass analyzers were adjusted to a resolution of 0.7 u full width at half height. For each spectrum, 9–150 continuum scans were averaged in multiple channel analyzer (MCA) mode. The source temperature (heated nebulizer) was 100 °C, the interface heater was on, +5.5 kV was applied to the electrospray capillary, the curtain gas was set at 20 (arbitrary units), and the two ion source gases were set at 45 (arbitrary units). The background of each spectrum was subtracted, the data were smoothed and peak areas were integrated using a custom script and Applied Biosystems Analyst software, and the data were corrected for overlap of isotopic variants (A + two peaks). A mass spectrum was acquired only on the internal standard mixture. Peaks corresponding to the target lipids in this spectrum were identified, and molar amounts were calculated in comparison with the two internal standards on the same lipid class. To correct for chemical or instrumental noise in the samples, the molar amount of each lipid metabolite detected in the internal-standards-only spectrum was subtracted from the molar amount of each metabolite calculated in each set of sample spectra. Finally, the data were corrected for the fraction of the sample analyzed, and the amount of each lipid species was divided by the total (× 100) to calculate molar percentage.

EM Analysis of Mdm12/Mmm1 Complexes and Molecular Modeling. Samples used for EM were purified as described previously with a final SEC purification performed in 50 mM NaCl, 20 mM Tris (pH 7.8). For negative-stain EM, a 2-μL sample was applied to a glow-discharged grid that was covered with carbon film. After 30-s incubation, the sample was blotted with filter paper and stained with 0.8% uranyl formate. EM micrographs were recorded on a TIETZ F415MP 16-megapixel CCD camera at 68,027× calibrated magnification in an FEI Tecnai F20 electron microscope operated at 200 kV. The micrographs were saved by 2× binning, yielding a pixel size of 4.41 Å. Image acquisition was performed with the assistance of Leginon automation software (10, 11). For RCT 3D reconstruction of Mdm12/Mmm1Δ5, micrographs were collected with the grids tilted at two angles successively (65° and 0°) for each specimen area of interest. For the other samples, micrographs were collected without tilting the grids. For RCT 3D reconstructions, corresponding particles (80 × 80 pixels) from each pair of tilted and untilted micrographs were picked using ApTiltPicker.py in Appion (12). To avoid bias in particle picking, all possible particles were picked for the following image classification. The defocus values of 0°-tilted and 65°-tilted micrographs were calculated by CTFFIND and CTFTILT programs (13), respectively. The phase flipping was performed on particle images before classification and 3D reconstructions. The 0°-tilted particles were classified using the Correspondence Analysis method in SPIDER (14). After classification, each class of 65°-tilted particles was subjected to 3D reconstruction using the Euler angles from both the geometrical relationship between the 65°-tilted and 0°-tilted images and the in-plane rotation alignment of the 0°-tilted images. The 3D RCT maps then were refined iteratively using the 65°-tilted particles with SPIDER by refinement of particle centers. No symmetry was applied during RCT 3D reconstruction and refinement. A representative 3D RCT map of Mdm12/Mmm1Δ5 was reconstructed at 35-Å resolution from 1,493 particles.

For 2D classification and 3D reconstruction of untilted images, particles (80 × 80 pixels) were picked automatically from micrographs using ApDogPicker.py in Appion. The phase flipping was performed on particle images using the defocus values estimated by CTFFIND. The 2D classification was performed using refine2d.py in EMAN (15). The 3D reconstruction and refinement of Mdm12/Mmm1Δ1 were carried out with EMAN using the 3D RCT map of Mdm12/Mmm1Δ5 as the starting model. Twofold symmetry was applied in the 3D refinement. The 3D map of Mdm12/Mmm1Δ1 was reconstructed at 17-Å resolution using 94,516 particles.

Molecular modeling and rigid body fitting were performed with COOT (16) and Chimera (17) for the final analysis, modeling, and rendering of the EM maps and complexes reconstructed by EM.

1. Suga H, et al. (2013) The Capsaspora genome reveals a complex unicellular prehistory of animals. *Nat Commun* 4:2325.
2. Kapust RB, Waugh DS (2000) Controlled intracellular processing of fusion proteins by TEV protease. *Protein Expr Purif* 19(2):312–318.
3. Li A, et al. (2008) Construction and characterization of bidirectional expression vectors in Saccharomyces cerevisiae. *FEMS Yeast Res* 8(1):6–9.
4. Maeda K, et al. (2013) Interactome map uncovers phosphatidylserine transport by oxysterol-binding proteins. *Nature* 501(7466):257–261.
5. Bligh EG, Dyer WJ (1959) A rapid method of total lipid extraction and purification. *Can J Biochem Physiol* 37(8):911–917.
6. Weerheim AM, Kolb AM, Sturk A, Nieuwland R (2002) Phospholipid composition of cell-derived microparticles determined by one-dimensional high-performance thin-layer chromatography. *Anal Biochem* 302(2):191–198.
7. Churchward MA, Brandman DM, Rogasevskaia T, Coorssen JR (2008) Copper (II) sulfate charring for high sensitivity on-plate fluorescent detection of lipids and sterols: Quantitative analyses of the composition of functional secretory vesicles. *J Chem Biol* 1(1-4):79–87.

8. Devaiah SP, et al. (2006) Quantitative profiling of polar glycerolipid species from organs of wild-type Arabidopsis and a phospholipase Dalpha1 knockout mutant. *Phytochemistry* 67(17):1907–1924.
9. Welti R, et al. (2002) Profiling membrane lipids in plant stress responses. Role of phospholipase D alpha in freezing-induced lipid changes in Arabidopsis. *J Biol Chem* 277(35):31994–32002.
10. Suloway C, et al. (2005) Automated molecular microscopy: The new Leginon system. *J Struct Biol* 151(1):41–60.
11. Suloway C, et al. (2009) Fully automated, sequential tilt-series acquisition with Leginon. *J Struct Biol* 167(1):11–18.
12. Lander GC, et al. (2009) Appion: An integrated, database-driven pipeline to facilitate EM image processing. *J Struct Biol* 166(1):95–102.
13. Mindell JA, Grigorieff N (2003) Accurate determination of local defocus and specimen tilt in electron microscopy. *J Struct Biol* 142(3):334–347.
14. Frank J, et al. (1996) SPIDER and WEB: Processing and visualization of images in 3D electron microscopy and related fields. *J Struct Biol* 116(1):190–199.
15. Ludtke SJ, Baldwin PR, Chiu W (1999) EMAN: Semiautomated software for high-resolution single-particle reconstructions. *J Struct Biol* 128(1):82–97.
16. Emsley P, Cowtan K (2004) Coot: Model-building tools for molecular graphics. *Acta Crystallogr D Biol Crystallogr* 60(Pt 12 Pt 1):2126–2132.
17. Pettersen EF, et al. (2004) UCSF Chimera—a visualization system for exploratory research and analysis. *J Comput Chem* 25(13):1605–1612.

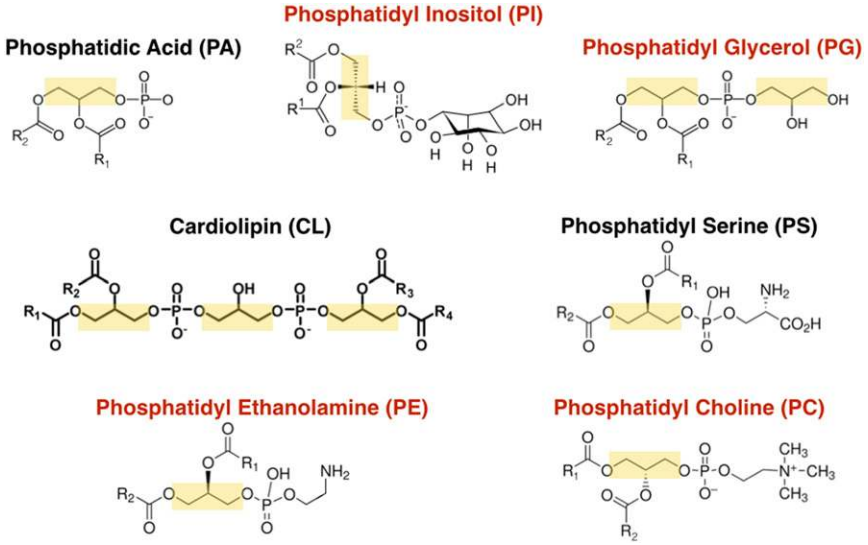

Fig. S1. Names, chemical structures, and abbreviations for the seven classes of common phosphoglycerolipids present in the ER and mitochondrial membranes.

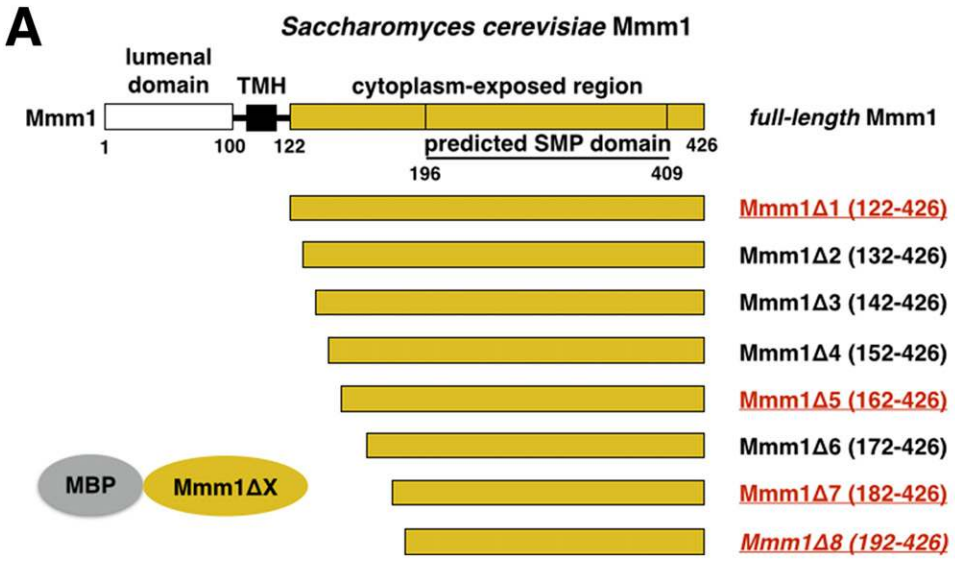

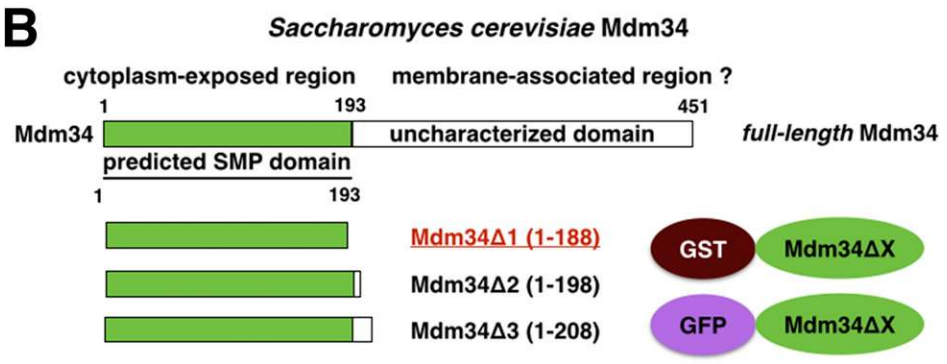

C

plasmid	cleavable tag	cleavable carrier	expression	use
Saccharomyces cerevisiae				
pCDF-Mdm12-his	both	-	single	lipid, EM & reconstitution
pCDF-Mdm12-his *S2G/W7A*	yes	-	single	reconstitution
pCDF-Mdm12-his *N142A/F148A*	yes	-	single	reconstitution
pCDF-Mdm12-flag	yes	-	coexpression	lipid, EM & reconstitution
pCDF-Mdm12-GFP-flag	no	no	coexpression	EM
pRSF-Mdm12-GFP-his	yes	no	single	crystallization
pRSF-Mmm1ΔX-his	yes	-	single & coexpression	lipid, EM & reconstitution
pRSF-MBP-Mmm1ΔX-his	yes both for Δ5	both	single & coexpression	lipid, EM & reconstitution
pRSF-MBP-Mmm1Δ5-his *E196A/N202A/Q207A*	yes	yes	single	reconstitution
pRSF-MBP-Mmm1Δ5-his *R373A/L376A/K381A*	yes	yes	single	reconstitution
pGEX4T1-Mdm34ΔX-his	yes	both	single & coexpression	lipid & reconstitution
pRSF-GFP-Mdm34ΔX-his	both	both	single & coexpression	lipid & reconstitution
pY23gpd-Mdm12-his	no	-	single	lipid
Saccharomyces castellii				
pRSF-his-MBP-Mdm12-his	yes	yes	single	lipid & reconstitution
pRSF-his-MBP-Mdm12-GFP-his	yes	MBP yes GFP no	single	reconstitution
Dictyostelium discoideum				
pRSF-his-MBP-Mdm12-his	yes	yes	single	lipid & reconstitution
pRSF-his-MBP-Mdm12-GFP-his	yes	MBP yes GFP no	single	reconstitution

Fig. S2. Mdm12 and Mmm1 expression constructs. (*A*) Nomenclature used for the truncation constructs of the *S. cerevisiae* Mmm1 protein. Eight deletion constructs mapping to the cytoplasmic domain of *Sce*-Mmm1 were generated through systematic deletion of10-residue increments starting at the N terminus of the predicted cytoplasmic domain of *Sce*-Mmm1. Construct Mmm1Δ1 (residues 122–426) encompasses the entire cytoplasmic domain. Residues 1–100 and 101–121 correspond to a glycosylated luminal domain and the single transmembrane-spanning helix, respectively. (*B*) Nomenclature used for the truncation constructs of the *S. cerevisiae* Mdm34 protein. Three deletion constructs mapping to the cytoplasmic domain of *Sce*-Mdm34 were generated through systematic deletion of 10-residue increments starting at the N terminus of the predicted cytoplasmic domain of *Sce*-Mdm34. (*C*) Summary of all protein constructs used in this study. ΔX refers to the deletion constructs Δ1 through Δ8 for Mmm1 and Δ1 through Δ3 for Mdm34; EM, structural EM with negatively stained samples of Mdm12/Mmm1 complexes; lipid, identification of bound lipids by MS and HPTLC; reconstitution, constructs used to produce Mdm12, Mdm34, and Mdm12/Mmm1 complexes used for the characterization and crystallization of ERMES.

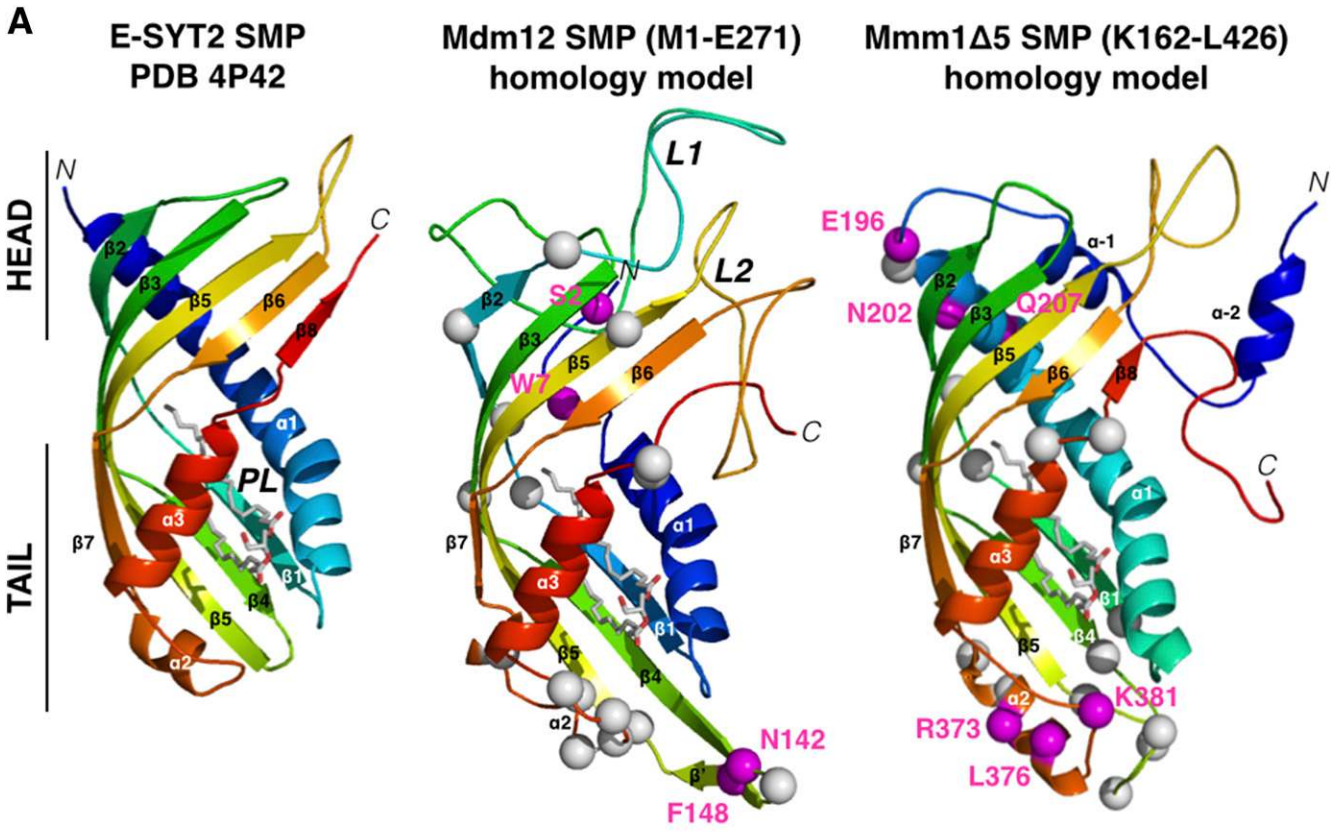

B

Phyre2 homology modeling: template ranking

Sce-Mdm12 full-length protein (residues M1-E271)					*Sce*-Mmm1Δ5 cytoplasmic fragment (residues K181-L146)				
Template PDB	Residues Modeled	% Confidence	% Sequence Identity	Raw Score	Template PDB	Residues Modeled	% Confidence	% Sequence Identity	Raw Score
4P42 [1]	7-269	99.7	18%	104.7	4P42 [1]	197-415	100	16%	200.8
2LCD	260-271	18.4	58%	14.6	2OBD [3]	218-401	84.5	12%	20.7
1EWF [2]	1-256	17	14%	13.5	1EWF [2]	218-401	68.8	17%	18.1
2ZU6	236-263	13.3	7%	14.2	4M4D [4]	218-401	43.6	21%	15.6
2ALJ	257-271	12.9	27%	13	1BP1 [2]	218-401	43	17%	15.6
2RG8	236-263	12.7	7%	14	3SQG	196-234	19.2	21%	13.7
3H2Z	227-260	11.4	9%	16.5	1LT1	162-208	18.1	25%	14.2
2OBD [3]	16-256	10.8	17%	12.5	1U7M	162-208	14.9	23%	14.6
1LJ8A	228-260	10.7	12%	12.5	3J1A	374-397	11.3	21%	12
4IM7	227-260	10.7	18%	12.5	2ROV	187-210	1	25%	12.5
3EIQ	236-263	10.3	7%	13.1					

Fig. S3. Phyre[2] homology modeling of the SMP domains in yeast Mdm12 and Mmm1. (*A*) The SMP domain crystal structure of E-SYT2 (PDB ID code 4P42) (1) was used to model the structures of yeast Mdm12 and Mmm1Δ5 in Phyre[2]. The structures in the ribbon diagram are shown in the same relative orientation with a bound phospholipid (PL) modeled. L1 (between strands β2 and β3) and L2 (between strands β5 and β6) correspond to the nonconserved insertions present in *S. cerevisiae* but not in *D. discoideum*. Residues with the highest degree of sequence conservation are represented by spheres. (*B*) Best structural templates identified by Phyre[2] for homology modeling. Template PDB is the crystal structure from the PDB used for sequence alignment and structure prediction by homology modeling. Residues modeled correspond to the region of the target protein (Mdm12 or Mmm1Δ5) that was modeled using the template structure from the PDB. % Sequence identity indicates the sequence identity between the query (Mdm12 or Mmm1Δ5) and the template PDB structure used for homology modeling. The model of Mdm12 has a 99.7% confidence score, with 67% of residues between residues W7 and G269 modeled at greater than 90% confidence. The model of Mmm1 has a confidence score of 100%, with 73% of the residues between residues S197 and S415 modeled at greater than 90% confidence. PDB ID codes: 1EWF and 1BP1, bactericidal permeability increase protein (2); 2OBD, cholesteryl ester transfer protein (3); 4M4D, lipopolysaccharide-binding protein (4).

1. Schauder CM, et al. (2014) Structure of a lipid-bound extended synaptotagmin indicates a role in lipid transfer. *Nature* 510(7506):552–555.
2. Beamer LJ, Carroll SF, Eisenberg D (1997) Crystal structure of human BPI and two bound phospholipids at 2.4 angstrom resolution. *Science* 276(5320):1861–1864.
3. Qiu X, et al. (2007) Crystal structure of cholesteryl ester transfer protein reveals a long tunnel and four bound lipid molecules. *Nat Struct Mol Biol* 14(2):106–113.
4. Eckert JK, et al. (2013) The crystal structure of lipopolysaccharide binding protein reveals the location of a frequent mutation that impairs innate immunity. *Immunity* 39(4):647–660.

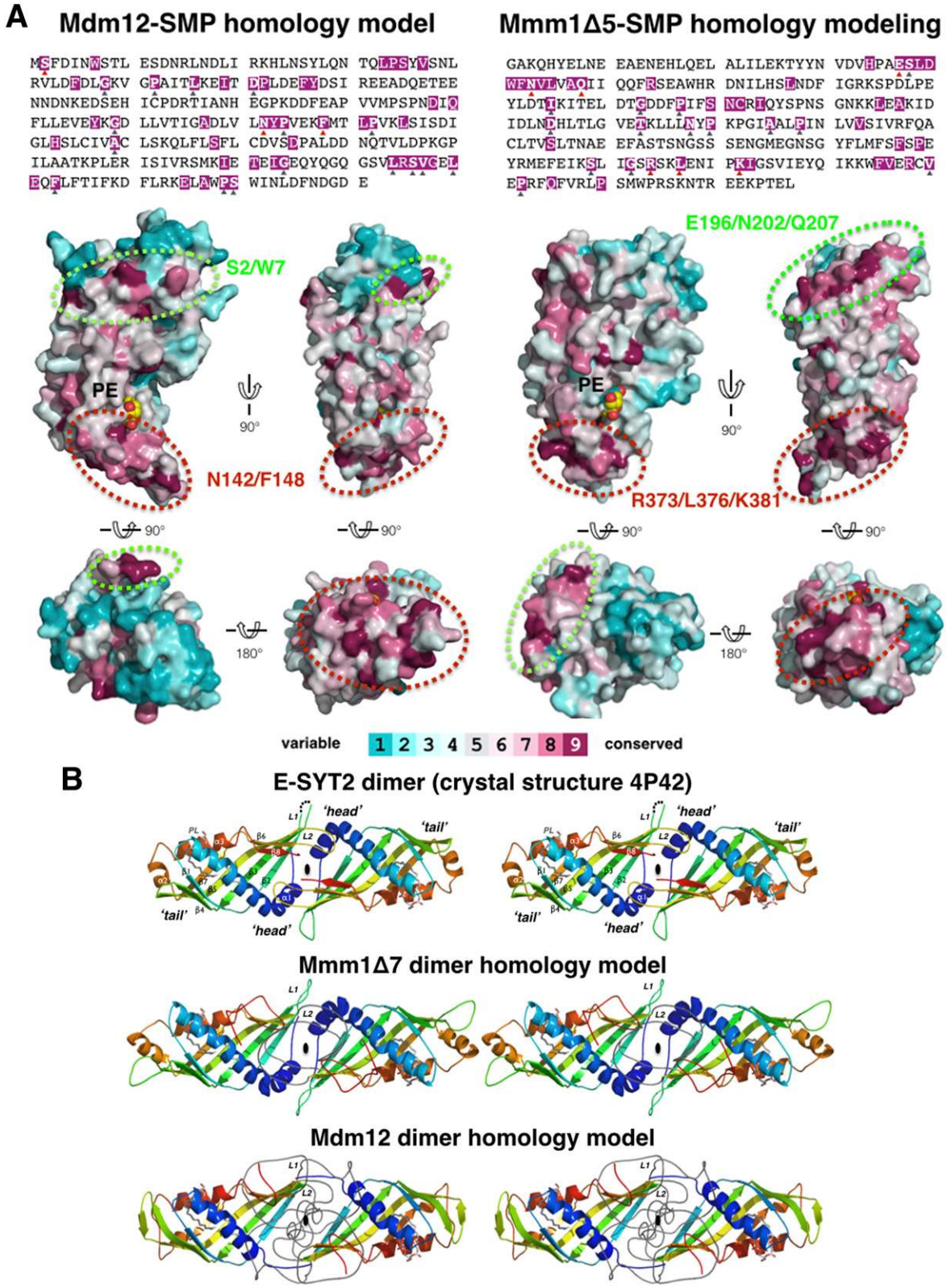

Fig. S4. Sequence conservation analysis in the SMP domains of Mdm12 and Mmm1. (*A*) The SMP domain crystal structure of E-SYT2 (PDB ID code 4P42) was used to model the structures of yeast Mdm12 and Mmm1Δ5 in Phyre[2]. Protein surfaces are colored according to sequence conservation as analyzed with ConSurf using the Mdm12 and Mmm1 protein sequences from 26 distinct organisms. Four different views of the two models are shown. A phospholipid (PL) has been modeled. Evolutionarily conserved protein surfaces are circled. (*B*) Homology models of Mdm12 and Mmm1Δ7 SMP domain homodimers. Stereoviews of the head-to-head E-SYT2 crystal structure used as a template to model putative SMP homodimers of Mmm1Δ7 and Mdm12. The two nonconserved large loops L1 and L2 of Mdm12 are next to the homodimerization interface described in E-SYT2. Secondary structure elements and loops L1 and L2 are labeled.

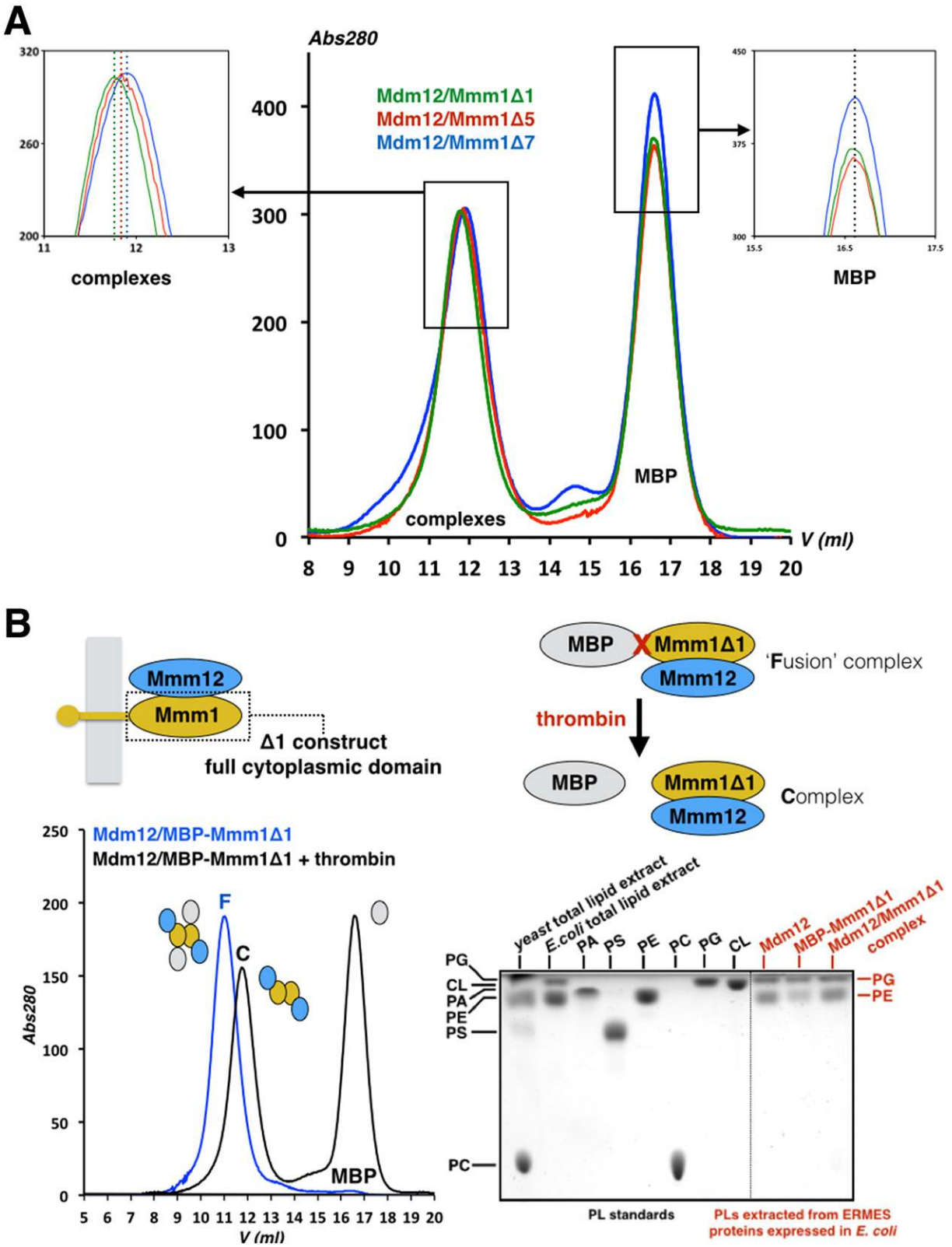

Fig. S5. Characterization of Mdm12/Mmm1ΔX complexes. (*A*) SEC comparative analysis of three Mdm12/Mmm1 complexes. Mdm12/Mmm1Δ1, Δ5, and Δ7 fusion complexes were treated with thrombin to release the MBP carrier, and the cleavage reaction was analyzed by SEC. *Insets* show the respective peaks with a perfect overlay of the severed MBP carrier (internal mass standard), but the three peaks corresponding to the three distinct native complexes are slightly shifted, reflecting the corresponding change in molecular weight. (*B*) The entire cytoplasmic domain of Mmm1 associates with Mdm12 to form a complex containing PE and PG. Shown is a simplified model of an Mdm12/Mmm1 subcomplex of yeast ERMES at the surface of the ER membrane. The Mmm1Δ1 construct encompasses the entire cytoplasmic domain of Mmm1. A fusion complex between Mdm12 and MBP-Mmm1Δ1 is coexpressed in *E. coli*. Upon treatment with thrombin, MBP is quantitatively released from the Mdm12/Mmm1Δ1 complex as shown by SEC. HPTLC analysis of the lipid content of Mdm12/MBP-Mmm1Δ1 complex shows that PG and PE are bound to protein.

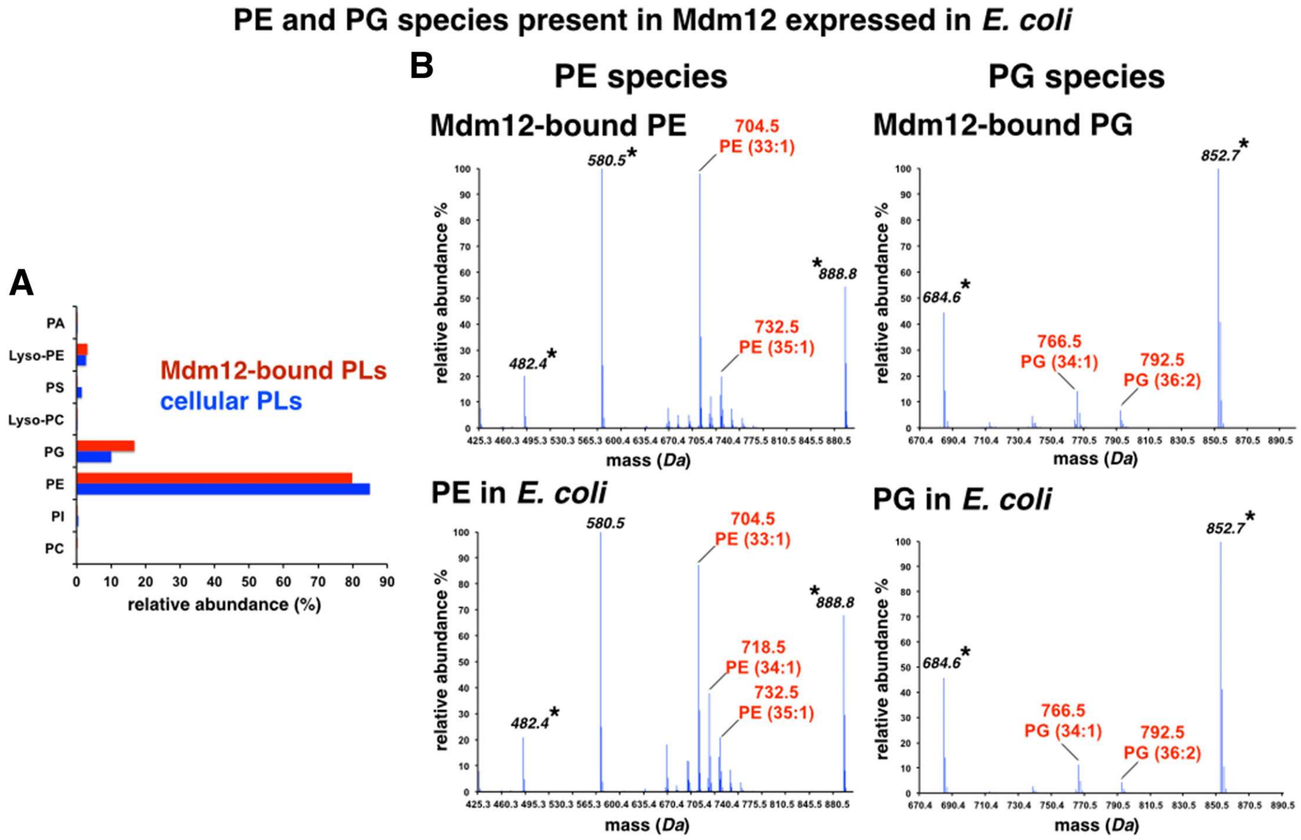

Fig. S6. Quantitative lipid profiling of Mdm12 purified from *E. coli* (heterologous expression) or yeast (homologous expression). Yeast Mdm12 expressed in *E. coli* promiscuously binds bacterial phospholipids PE and PG. (*A*) Comparative analysis of phospholipids present in bacteria (blue bars) and phospholipids bound to Mdm12 (red bars). The observed ratio of PE/PG bound to Mdm12 matches their natural relative abundance in bacteria (PE ~85%; PG ~10%). (*B*) ESI-MS reveals a broad spectrum of PE and PG species bound to Mdm12 (*Upper*) and normally present in bacteria (*Lower*). The main PE species bound to Mdm12 is PE(33:1) with a mass of 704.5 Da. The main PG species bound is PG(34:1) with a mass of 766.5 Da. Yeast Mdm12 preferentially binds PC in vivo. (*C*) ESI-MS reveals a broad spectrum of PC species tightly bound to Mdm12 purified from yeast (*Left*) and PC species present in total yeast lipids (*Right*). Of the bound PC, Mdm12 is specifically enriched by at least twofold with species PC(32:2) (mass of 730.5 Da), compared with the natural abundance of the same species in yeast. Other PC species present are labeled in red. Phospholipid internal standards are indicated by an asterisk.

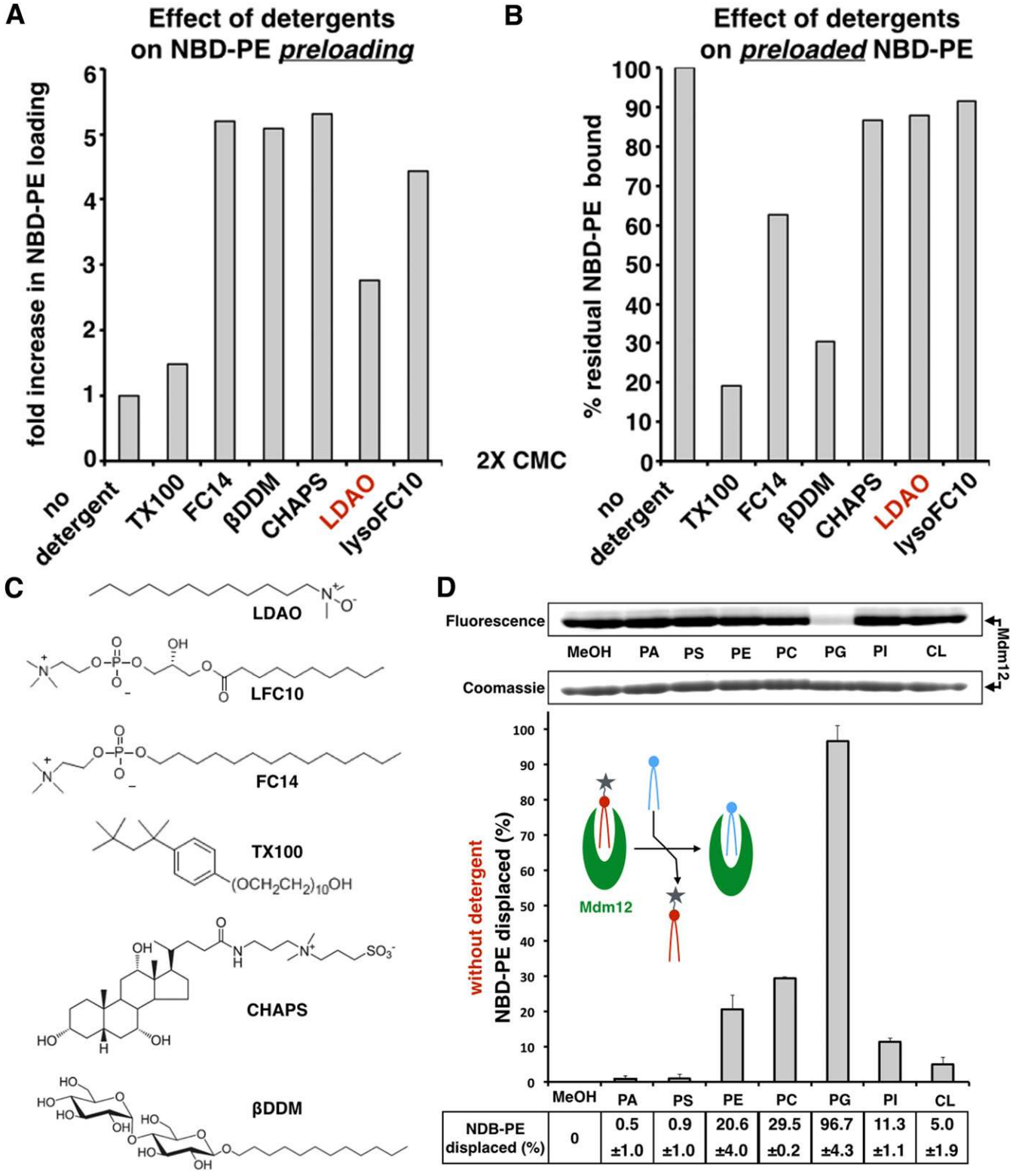

Fig. S7. Effects of detergents on lipid displacement in Mdm12. (*A*) Detergent-facilitated preloading of NBP-PE in Mdm12. (*B*) Detergent-induced displacement of NBP-PE preloaded in Mdm12. (*C*) Structures and CMCs of the six detergents used in lipid displacement assays. (*D*) Lipid displacement assay in the absence of detergent.

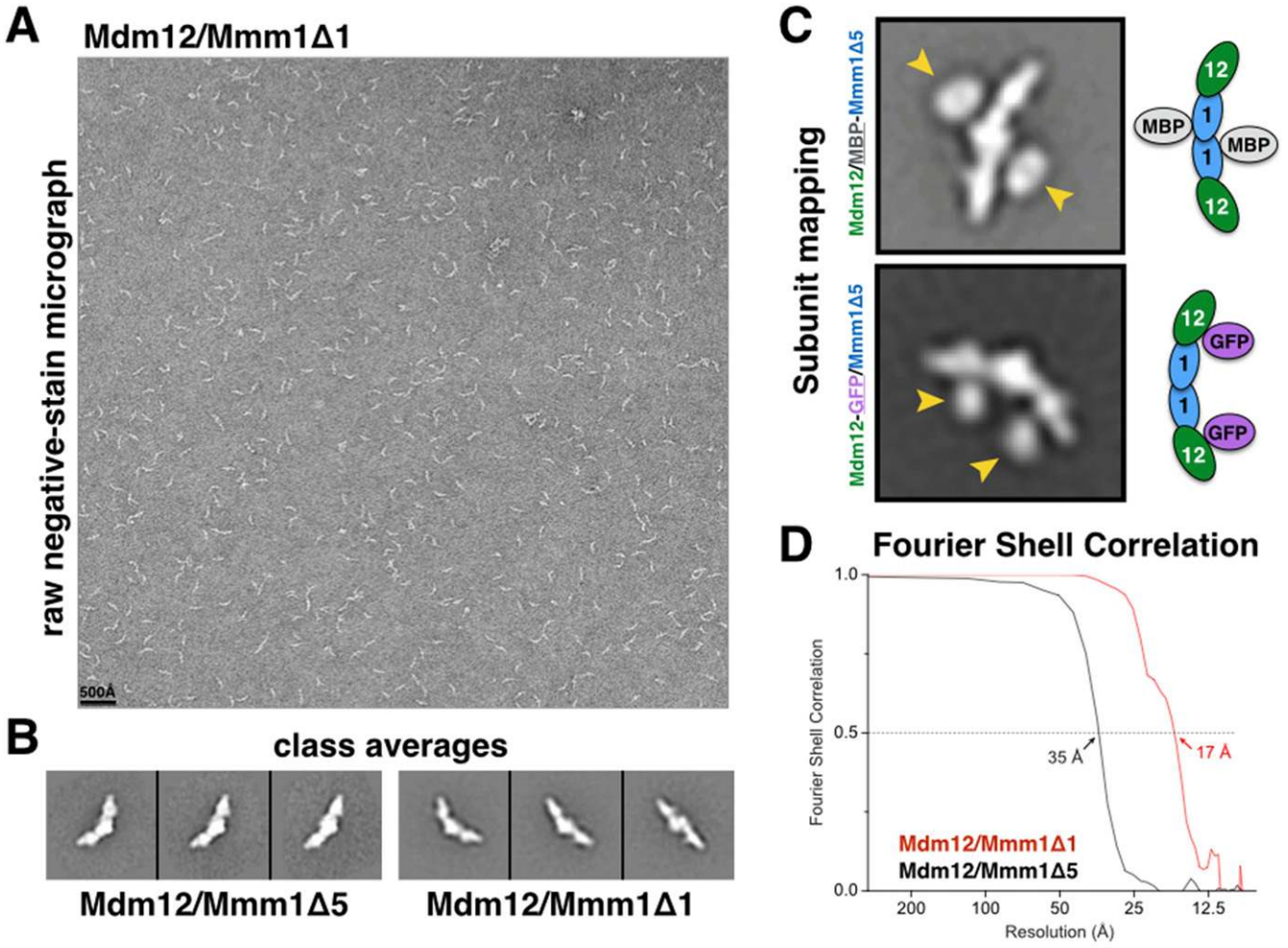

E

Reconstruction method	Untilted		Random Conical Tilt (RCT)	
Sample	Micrograph count	Particle count	Micrograph pair count	Particle count
Mdm12/Mmm1Δ5	-	-	**606**	**61,822**
Mdm12/Mmm1Δ1	**199**	**94,516**	-	-
Mdm12/MBP-Mmm1Δ5	388	83,072	-	-
Mdm12-GFP/Mmm1Δ5	214	80,341	-	-
Mdm12/MBP-Mmm1Δ1	236	84,531	-	-

Fig. S8. Negative-stain EM analyses of Mdm12/Mmm1 complexes. (*A*) Representative raw negative-stain EM micrograph of an Mdm12/Mmm1Δ1 complex. The 500-Å scale bar corresponds to 113 pixels of 4.41 Å. (*B*) Representative class averages obtained for Mdm12/Mmm1Δ1 and Mdm12/Mmm1Δ5 complexes. (*C*) Subunit mapping using N-terminal MBP and C-terminal GFP fusion tags for Mmm1 and Mdm12, respectively. (*D*) Fourier shell correlation (FSC) of the RCT 3D reconstructions of the Mdm12/Mmm1Δ5 complex (black trace) and of the refined 3D reconstruction of the Mdm12/Mmm1Δ1 complex using untilted particle images and with twofold symmetry (red trace). Resolutions are estimated at the FSC = 0.5 criterion. (*E*) Summary of the samples used in the EM analyses.

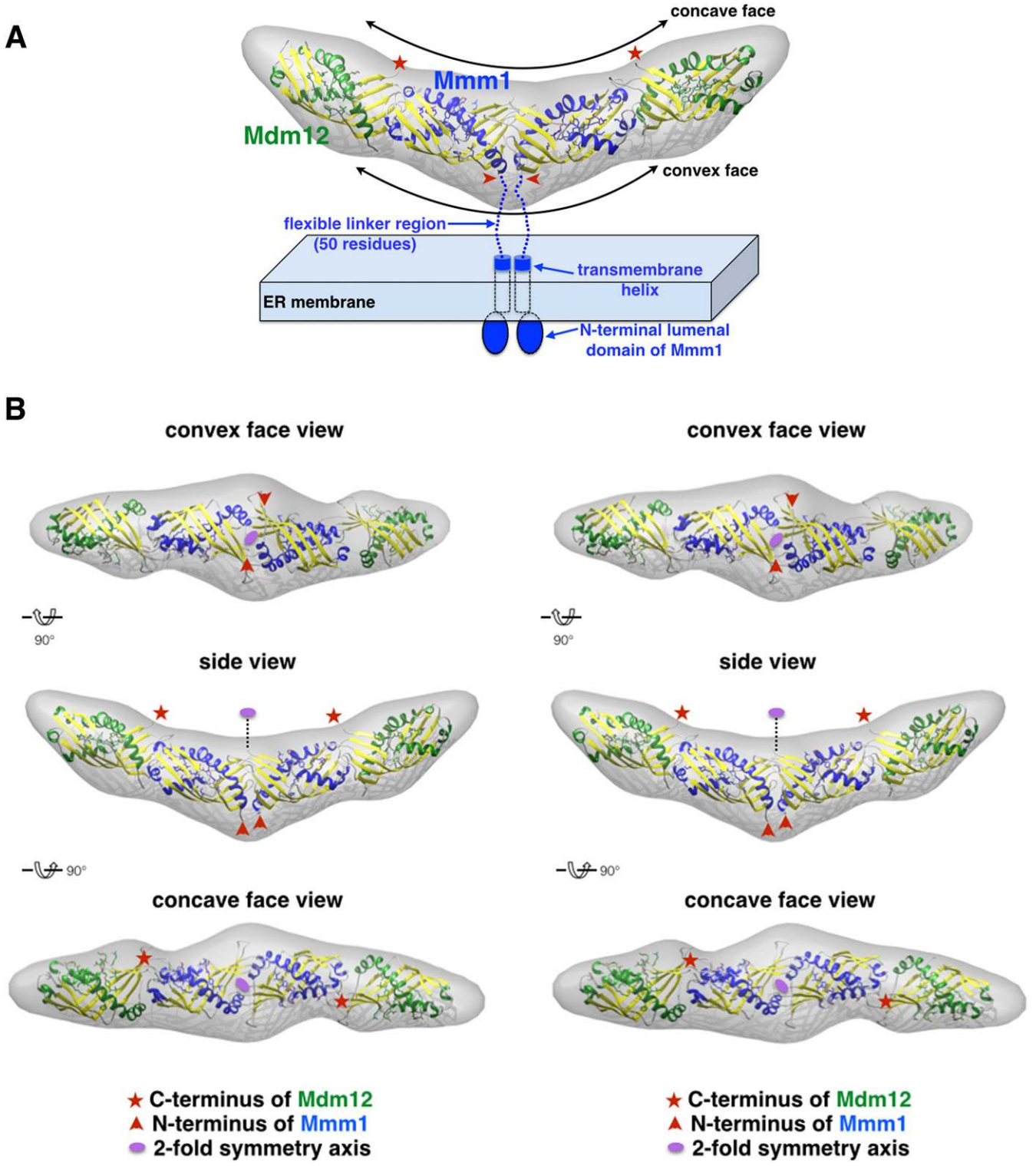

Fig. S9. Architecture of the Mdm12/Mmm1 complex. (*A*) Schematic showing the model of the Mdm12/Mmm1 subcomplex at the ER surface based on our EM analysis. (*B*) Stereoviews of the convex face, concave face, and side of the complex. The positions of the N terminus of Mmm1 (red arrowheads) and C terminus of Mdm12 (red stars) are highlighted and agree with the EM class averages obtained using MBP-Mmm1 or Mdm12-GFP fusion-based complexes (Fig. 7 *A*–*C* and Fig. S8*C*). The twofold axis of symmetry is indicated also.

Table S1. MS profiling of phospholipids bound to yeast Mdm12 purified from yeast or *E. coli*

m/z	Species	
PC bound to Mdm12 purified from yeast		
648.5	C34H66O8PN	PC(26:1)
650.5	C34H68O8PN	PC(26:0)
676.5	C36H70O8PN	PC(28:1)
678.5	C36H72O8PN	PC(28:0)
702.5	C38H72O8PN	PC(30:2)
704.5	C38H74O8PN	PC(30:1)
706.5	C38H76O8PN	PC(30:0)
716.5	C39H74O8PN	PC(31:2)
718.5	C39H76O8PN	PC(31:1)
730.5	**C40H76O8PN**	**PC(32:2)**
732.5	**C40H78O8PN**	**PC(32:1)**
744.5	C41H78O8PN	PC(33:2)
746.6	C41H80O8PN	PC(33:1)
748.6	C41H82O8PN	PC(33:0)
756.5	C42H78O8PN	PC(34:3)
758.6	C42H80O8PN	PC(34:2)
760.6	C42H82O8PN	PC(34:1)
786.6	C44H84O8PN	PC(36:2)
788.6	C44H86O8PN	PC(36:1)
PE bound to Mdm12 purified from *E. coli*		
634.4	C33H64O8PN	PE(28:1)
662.5	C35H68O8PN	PE(30:1)
664.5	C35H70O8PN	PE(30:0)
676.5	C36H70O8PN	PE(31:1)
678.5	C36H72O8PN	PE(31:0)
688.5	C37H70O8PN	PE(32:2)
690.5	C37H72O8PN	PE(32:1)
692.5	C37H74O8PN	PE(32:0)
702.5	C38H72O8PN	PE(33:2)
704.5	**C38H74O8PN**	**PE(33:1)**
716.5	C39H74O8PN	PE(34:2)
718.5	**C39H76O8PN**	**PE(34:1)**
720.5	C39H78O8PN	PE(34:0)
730.5	**C40H76O8PN**	**PE(35:2)**
732.5	**C40H78O8PN**	**PE(35:1)**
744.5	C41H78O8PN	PE(36:2)
746.6	C41H80O8PN	PE(36:1)
758.6	C42H80O8PN	PE(37:2)
760.6	C42H82O8PN	PE(37:1)
772.6	C43H82O8PN	PE(38:2)
PG bound to Mdm12 purified from *E. coli*		
710.5	C36H69O10P	PG(30:1)
712.5	C36H71O10P	PG(30:0)
736.5	C38H71O10P	PG(32:2)
738.5	**C38H73O10P**	**PG(32:1)**
740.5	C38H75O10P	PG(32:0)
764.5	**C40H75O10P**	**PG(34:2)**
766.5	**C40H77O10P**	**PG(34:1)**
792.5	**C42H79O10P**	**PG(36:2)**
794.6	C42H81O10P	PG(36:1)

The most abundant phospholipid species are in bold.

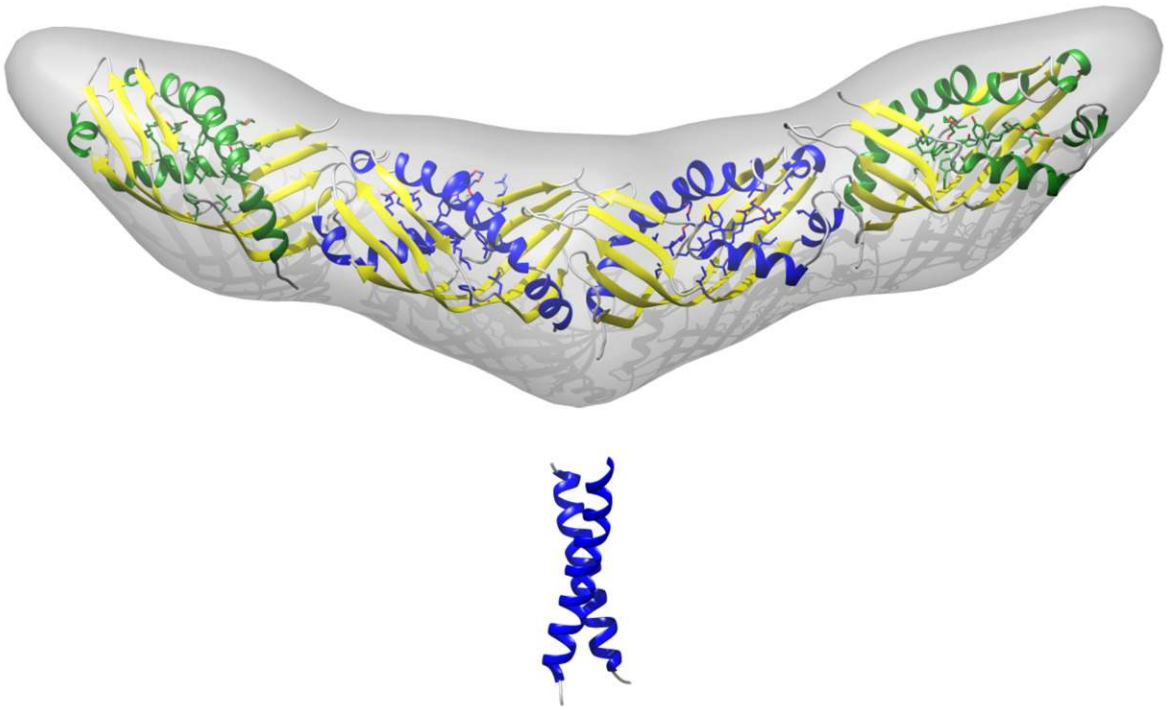

Movie S1. Fitting of four SMP domains in the 17-Å-resolution EM-density map of the Mdm12/Mmm1Δ1 heterotetramer. Four E-SYT2 SMP domains were docked in the EM map. SMP domains corresponding to Mdm12 subunits are colored in green (helices) and yellow (strands). SMP domains corresponding to Mmm1 subunits are colored in blue (helices) and yellow (strands). Two α-helices, each corresponding to the single transmembrane helix present in Mmm1, are shown. The EM-density map is represented as a transparent gray envelope.

Movie S1

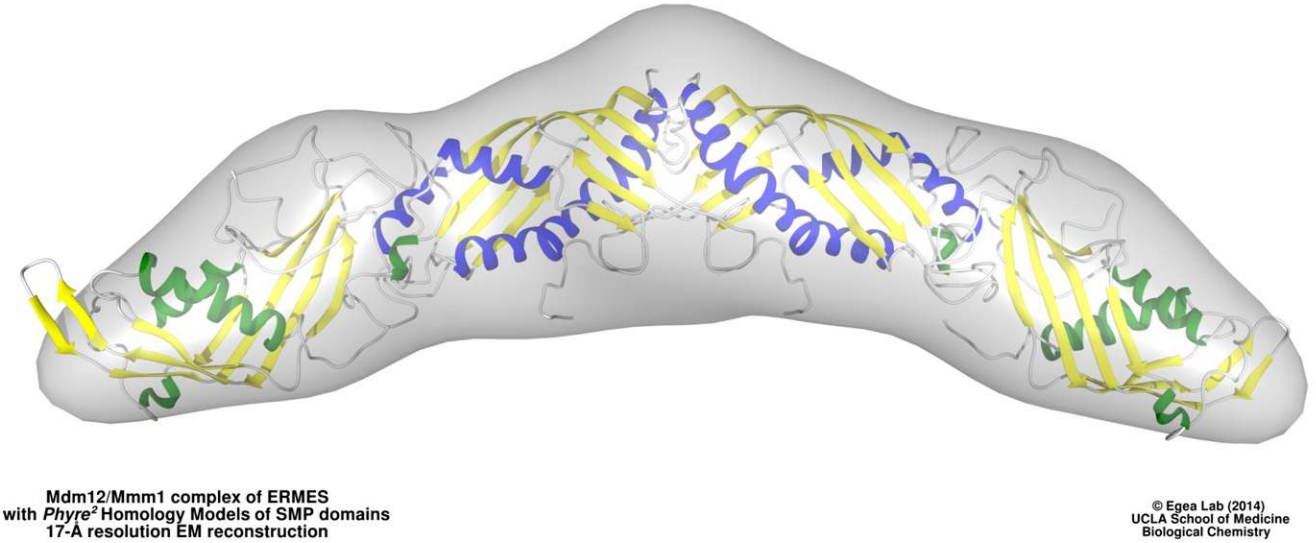

Movie S2. Mdm12/Mmm1 ERMES complex homology model derived from the 17-Å-resolution EM reconstruction. The homology models of Mdm12 (monomer) (Fig. 1*C*) and Mmm1 (dimer) (Fig. S4*B*) were used to generate a model of the Mdm12/Mmm1 complex. Mdm12 subunits are colored in green (helices) and yellow (strands). Mmm1 subunits are colored in blue (helices) and yellow (strands). The EM-density map is represented as a transparent gray envelope. A scale bar is shown.

Movie S2